Transfer-printed, tandem microscale light-emitting diodes for full-color displays

Lizhu Li[a], Guo Tang[a], Zhao Shi[a], He Ding[b], Changbo Liu[c], Dali Cheng[a], Qianyi Zhang[d], Lan Yin[d], Zhibo Yao[e], Lian Duan[e], Donghao Zhang[f], Chenggong Wang[f], Meixin Feng[g], Qian Sun[g], Qiang Wang[a], Yanjun Han[a], Lai Wang[a], Yi Luo[a], and Xing Sheng (盛兴)[a,1]

[a]Department of Electronic Engineering, Beijing National Research Center for Information Science and Technology, Center for Flexible Electronics Technology, Tsinghua University, 100084 Beijing, China; [b]Beijing Engineering Research Center of Mixed Reality and Advanced Display, School of Optics and Photonics, Beijing Institute of Technology, 100081 Beijing, China; [c]School of Materials Science and Engineering, Beihang University, 100191 Beijing, China; [d]School of Materials Science and Engineering, Tsinghua University, 100084 Beijing, China; [e]Department of Chemistry, Tsinghua University, 100084 Beijing, China; [f]R&D Department, Chengdu Vistar Optoelectronics Co., Ltd., 611730 Chengdu, China; and [g]Suzhou Institute of Nano-Tech and Nano-Bionics, Chinese Academy of Sciences (CAS), 215123 Suzhou, China

Inorganic semiconductor-based microscale light-emitting diodes (micro-LEDs) have been widely considered the key solution to next-generation, ubiquitous lighting and display systems, with their efficiency, brightness, contrast, stability, and dynamic response superior to liquid crystal or organic-based counterparts. However, the reduction of micro-LED sizes leads to the deteriorated device performance and increased difficulties in manufacturing. Here, we report a tandem device scheme based on stacked red, green, and blue (RGB) micro-LEDs, for the realization of full-color lighting and displays. Thin-film micro-LEDs (size ~100 μm, thickness ~5 μm) based on III–V compound semiconductors are vertically assembled via epitaxial liftoff and transfer printing. A thin-film dielectric-based optical filter serves as a wavelength-selective interface for performance enhancement. Furthermore, we prototype arrays of tandem RGB micro-LEDs and demonstrate display capabilities. These materials and device strategies provide a viable path to advanced lighting and display systems.

light-emitting diodes | micro-LEDs | transfer printing | displays | optical filters

Microscale light-emitting diodes (micro-LEDs) based on inorganic semiconductors have been widely regarded as one of the most promising solutions to the next generation of emissive display technologies for versatile applications, from televisions, smartphones and wearable watches, to advanced virtual, augmented, and mixed realities (1–4). Constructed from single-crystalline–compound semiconductors like gallium arsenide (GaAs), gallium phosphide (GaP), and gallium nitride (GaN), these micro-LEDs present significant benefits over conventional liquid crystal displays (LCDs) (5), organic LEDs (OLEDs) (6–9), and more recent quantum dot (10, 11) and perovskite-based LEDs (12), in terms of their efficiencies, brightness, contrast, dynamic response, and long-time stability. High-resolution displays rely on arrays of polychromatic (red, green, and blue [RGB]) emissive elements with dimensions of less than 100 μm or even 10 μm, which are massively and heterogeneously assembled onto silicon, glass, or plastic substrates (13–17). This scaling down of device sizes enhances the display resolution and reduces the raw material cost; however, it is also accompanied by significant challenges. First, reducing LED size causes dramatic efficiency decreases for all types of LEDs (18–21), particularly GaAs- or GaP-based red LEDs that are more susceptible to sidewall defects (*SI Appendix*, Fig. S1). Second, device shrinkage also results in deteriorated uniformity, which influences the reliability and performance of display systems. Third, fabricating and transferring smaller devices demand higher accuracies for alignment and positioning (22), imposing greatly increased manufacturing expenses (*SI Appendix*, Fig. S2).

Alternatively, device arrays with a single-pixel, spectrally tunable LED (23) or vertically stacked tandem LEDs (24) relieve the above constraints associated with conventional laterally arranged RGB micro-LEDs. However, color-tunable LEDs based on voltage-dependent spectral change can neither achieve full-range tunability nor obtain independent color/intensity controllability (25, 26). On the other hand, the current state-of-the-art wafer-bonding–based assembly methods only realize double-layer stacking with the capability of dual-color tuning (green/blue or red/blue) (22, 27, 28). Although there are some reports on full-color stacked inorganic and organic RGB LEDs (24, 29–31), these demonstrations are only limited to a few of chip-scale, large or thick LEDs for lighting purposes.

In this paper, we report a tandem thin-film RGB micro-LED architecture with full-range color tunability to overcome the limitations of previously explored technologies. Based on the epitaxial liftoff and transfer printing method, arrays of thin-film, high-performance, inorganic RGB micro-LEDs made of different III–V compounds are assembled in a vertical stack. Embedded into the stacked structure, a thin-film dielectric filter serves as a wavelength selective interlayer to improve the LED light output. Independently addressable active arrays show full-color electroluminescent patterns, demonstrating the display capability of the tandem micro-LEDs.

Significance

Inorganic semiconductor based micro-LEDs have recently attracted tremendous interests of both industrial developers and academic researchers for the realization of next-generation displays. The reduction of LED sizes causes performance degradation and increased fabrication challenges. In this paper, we introduce a tandem device scheme based on stacked red, green, and blue (RGB) micro-LEDs for the realization of full-color lighting and displays. Thin-film micro-LEDs (size ~100 μm, thickness ~5 μm) based on III–V compound semiconductors are vertically assembled via epitaxial liftoff and transfer printing. A thin-film dielectric-based optical filter serves as a wavelength selective interface for performance enhancement. Furthermore, we prototype arrays of tandem RGB micro-LEDs and demonstrate display capabilities across the entire visible wavelength range.

ENGINEERING

Results

Fig. 1*A* schematically illustrates and compares laterally arranged RGB micro-LED arrays and vertically stacked, tandem arrays. To realize the same resolution (or pixels per inch, PPI) for display purposes, the minimum required LED size in the tandem design can be three times larger than that in the lateral arrangement structure. As described in aforementioned discussions and *SI Appendix*, Figs. S1 and S2, the use of larger LEDs holds the advantages of enhanced device performance and reduced nonuniformity as well as higher tolerance to alignment errors during microfabrication and device placement. The exploded cartoon image of our tandem micro-LED array and pixel design is depicted in Fig. 1*B*. Details of fabrication are described in the *SI Appendix*, Figs. S3–S9 and Tables S1–S4. From top to bottom, a single pixel comprises an indium gallium nitride (InGaN) blue LED, an InGaN green LED, a longpass band selective filter, and an indium gallium phosphide (InGaP) red LED. The designed epitaxial structures of these blue, green, and red LEDs are adopted from the standard multiple quantum wells incorporating emissive layers made of $In_{0.15}Ga_{0.85}N$, $In_{0.3}Ga_{0.7}N$, and $In_{0.5}Ga_{0.5}P$, respectively, as well as cladding layers (32). In particular, a distributed Bragg reflector is designed within the red LED for improved light extraction (35). These thin-film–based, microscale devices are epitaxially grown and lithographically fabricated on rigid, single-crystalline wafers (sapphire for InGaN blue and green LEDs and GaAs for InGaP red LEDs and filters) and subsequently separated from original substrates by laser liftoff (for

sapphire) (33, 34) or selective etching (for GaAs) (13, 35–37). Optical images and electroluminescence (EL) spectra of individual RGB micro-LEDs are provided in *SI Appendix*, Fig. S6, showing EL emission peaks at 628 nm, 530 nm, and 475 nm for RGB LEDs, respectively. Released, freestanding thin-film devices are transfer printed onto foreign rigid (e.g., glass) or flexible (e.g., polyimide) substrates (38, 39), forming a vertically assembled stack. In such a tandem structure, RGB micro-LEDs share the same geometries and are accurately overlaid. In addition, the designed optical filter layer between the red and green LEDs offers not only high transmission for red light but also a near-unity reflectivity at shorter wavelengths (<600 nm), increasing the light extraction for blue and green LEDs. Most active layers (GaN, ITO, etc.) in the blue and green LEDs are inherently transparent in the visible range, further minimizing the optical losses for red light emitted from the bottom InGaP LED. The active InGaN emitter (thickness ~20 nm in the quantum wells) in the green LED only slightly absorbs blue light (with an optical loss around 10% at 475 nm) (40). Besides, the large spectral overlap of the blue and green LEDs makes the design of a filter layer for optimized reflection (for blue) and transmission (for green and red) difficult and unnecessary. Irradiations from the RGB micro-LEDs in a tandem stack with a thin-film filter are schematically illustrated in *SI Appendix*, Fig. S10. Different device layers are separated by SU-8 epoxy–based thin films, which serve as electrically insulating, optically transparent, and mechanically adhesive bonding interfaces. During the transfer process, these heterogeneously
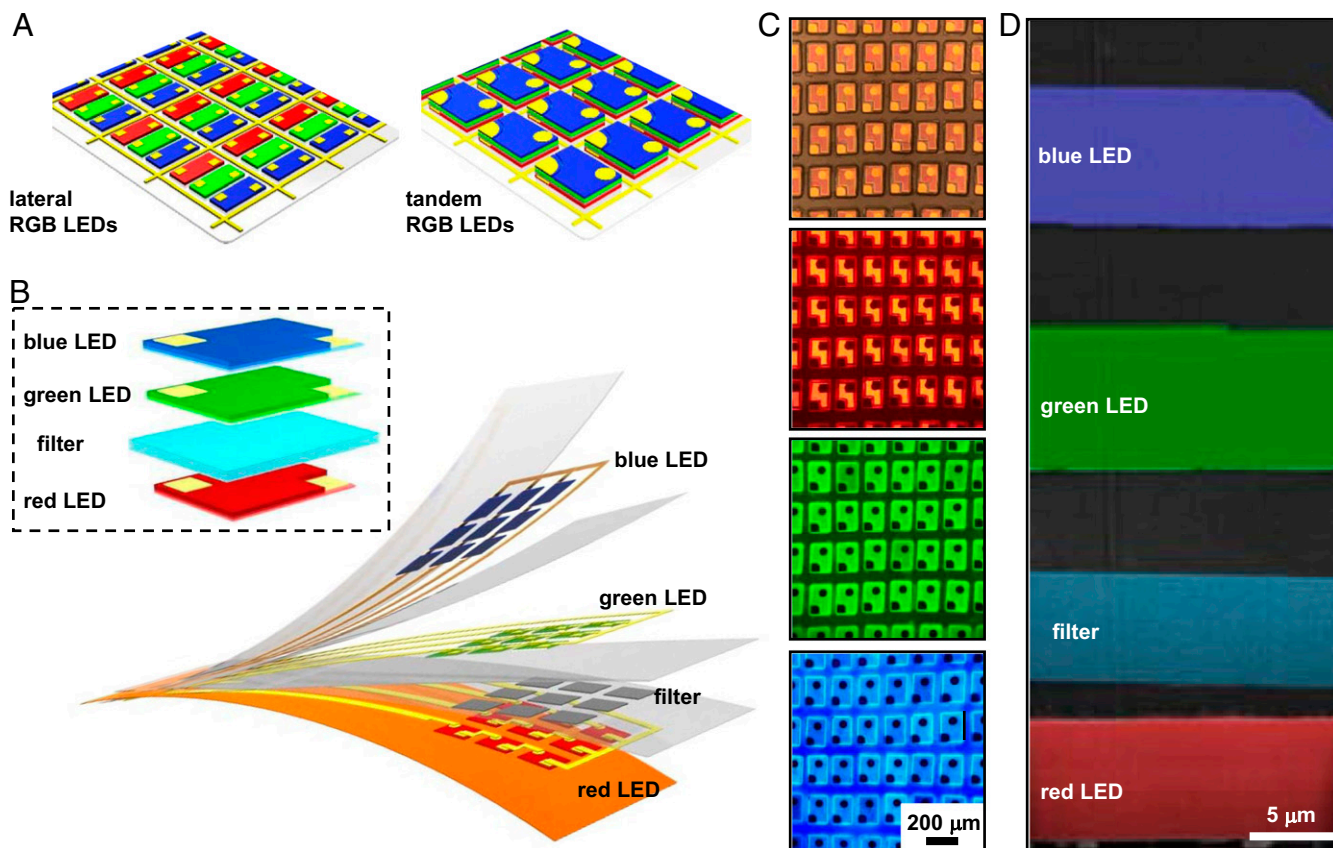

Fig. 1. Schematic illustrations and images of tandem RGB thin-film micro-LEDs and device arrays, assembled by the transfer printing method. (*A*) Comparison of a conventional parallel RGB micro-LED array (*Left*) and our proposed tandem RGB micro-LED array (*Right*), with the same display resolution. (*B*) Exploded schematic of tandem RGB micro-LED arrays, with the inset showing a single pixel, comprising an InGaP red LED, a multilayer SiO₂/TiO₂ filter, an InGaN green LED, and an InGaN blue LED (from bottom to top). The stacked devices can be assembled on various substrates. (*C*) Fluorescent microscopic images for an array of tandem RGB micro-LEDs. From top to bottom: bright field view, RGB emissions under green/blue/ultraviolet (UV) illuminations, respectively. (*D*) Cross-sectional scanning electron microscope (SEM) image of tandem RGB micro-LEDs with colorized regions showing thin films of RGB micro-LEDs as well as the filter interlayer. Different device layers are separated by layers of SU-8 epoxy.

integrated micro-LEDs can be further metalized to form electrically-driven emissive arrays for display applications (schematically illustrated in Fig. 1*B*). Fig. 1*C* illustrates a representative array (more than 6 × 8 pixels) of tandem RGB micro-LEDs printed onto a polyimide substrate without metal lines. Fluorescence images captured at various spectral ranges clearly reveal photoluminescent emission from the RGB LEDs, indicating that these micro-LEDs are well positioned with minimal misalignments. Although each micro-LED has a lateral dimension around 125 μm × 180 μm, the presented tandem array holds a resolution that is identical to a conventional lateral RGB array with LED sizes three times smaller (around 125 μm × 60 μm). Display systems based on arrays of such a tandem RGB pixel can reach a PPI of 200 to 400, which is higher than state-of-the-art high-definition televisions and on a par with those in smartphones. The scanning electron microscope (SEM) image in Fig. 1*D* presents the cross-sectional structure of a tandem RGB micro-LED. Thin-film RGB LEDs and the filter have thicknesses around 5 to 7 μm, with 2 to 5 μm thick SU-8 epoxy interlayers between each device, resulting in a total thickness of around 45 μm. Shown in the SEM image, the tilted device layers are mainly attributed to the nonuniformity of the organic adhesive (SU-8 epoxy), which can be addressed by reducing the adhesive thickness and optimizing the baking and transfer processes.

The separated metallization for RGB micro-LEDs in the tandem structure allows independent electrical control of individual devices. Fig. 2 *A–C* plot micrographs and measured EL spectra for RGB micro-LEDs in the tandem structure. The emission spectra are identical to those for micro-LEDs on original substrates (*SI Appendix*, Fig. S6), showing that these micro-LEDs in the tandem design can work independently with negligible electrical or optical crosstalk. Continuously adjustable currents can be injected into two or three micro-LEDs in the stack, and the combined spectra realize emissions of different colors like white, cyan, yellow, and purple (Fig. 2 *D–G*). Dynamic color change is also captured and shown in Movie S1. The color space achieved by our tandem micro-LED emitter is provided in Fig. 2*H*, which has a 93% overlap with the Adobe RGB color gamut within the CIE 1931

chromaticity diagram by the International Commission for Illumination (Commission International de L'Eclairage, CIE) (32). Coordinates for various EL spectra presented in Fig. 2 *D–G* are also indicated in Fig. 2*H*, which are (0.68, 0.30), (0.24, 0.72), (0.12, 0.14), (0.33, 0.33), (0.16, 0.36), (0.49, 0.48), (0.39, 0.23) for red, green, blue, white, cyan, yellow, and purple emissions, respectively. These results clearly demonstrate the capability of full-color coverage within the visible range for display applications.

To offer a proof of concept, we prepare arrays of tandem RGB micro-LEDs metalized with independent electrical contact pads for active display demonstrations in Fig. 3. Fig. 3*A* presents a pixel array to realize a simple seven-segment display, which is able to dynamically output decimal digits from 0 to 9 with various colors (*SI Appendix*, Fig. S11 and Movie S2). Additionally, Fig. 3*B* shows a device array with 3 × 3 pixels displaying different colored patterns (*SI Appendix*, Fig. S12 and Movie S3). The overall yield for micro-LED fabrication, transfer, stacking, and interconnection can reach nearly 100% for these small-scale arrays. The tandem design has the potential to be expanded for large-scale emissive arrays, leveraged by automated, massive transfer technique (41) and advanced driver circuits with matrix-addressable functions (2, 42).

Fig. 4 and Table 1 summarize the measured optoelectronic performance for RGB micro-LEDs in a representative, complete tandem stack. Current and voltage characteristics in Fig. 4*A* show threshold voltages of about 1.6 V, 2.2 V, and 2.4 V, and currents reaching 10 mA at 2.5 V, 2.6 V, and 2.9 V for red, green and blue micro-LEDs, respectively. Compared to unreleased micro-LEDs on original growth substrates, performances for these devices in the tandem structure do not experience degradations after wafer separation and transfer printing. Furthermore, the results verify that the tandem device configuration do not induce unwanted interferences among the individual micro-LEDs. For all the micro-LEDs, measured luminance levels are in the range of 1 to 10 cd/mm² at injected currents of 1 to 10 mA (Fig. 4*B*). The performances are similar to those for previously reported inorganic micro-LEDs (in the order of 10^6 to 10^7 cd/m²) (3, 15, 43) and much higher than those reported OLEDs (10^3 to 10^4 cd/m²)
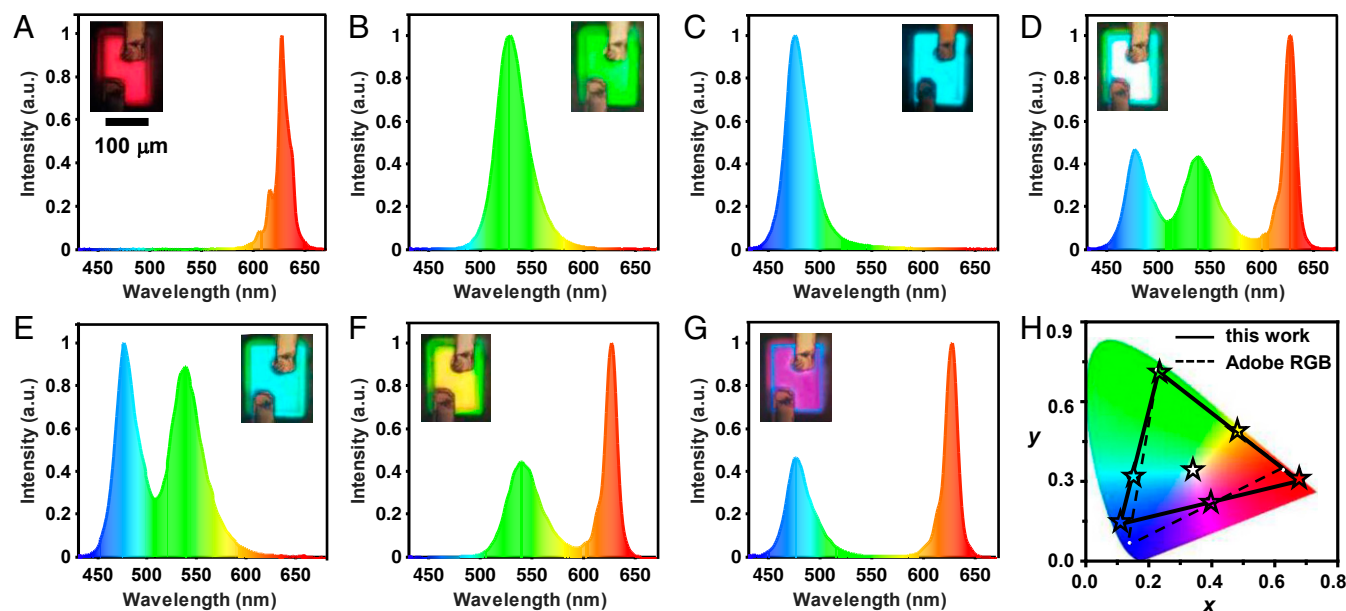

Fig. 2. Optical micrographs and EL performance of tandem RGB micro-LEDs. (*A–G*) EL spectra of a tandem device when currents are injected into different LEDs. Insets show optical images displaying different colors: (*A*) red, (*B*) green, (*C*) blue, (*D*) white, (*E*) cyan, (*F*) yellow, and (*G*) purple. (*H*) Chromaticity of tandem RGB micro-LEDs (solid line) in the CIE1931 color space, comparing with the Adobe RGB (dashed line). The stars represent the coordinates for spectra measured in *A–G*.
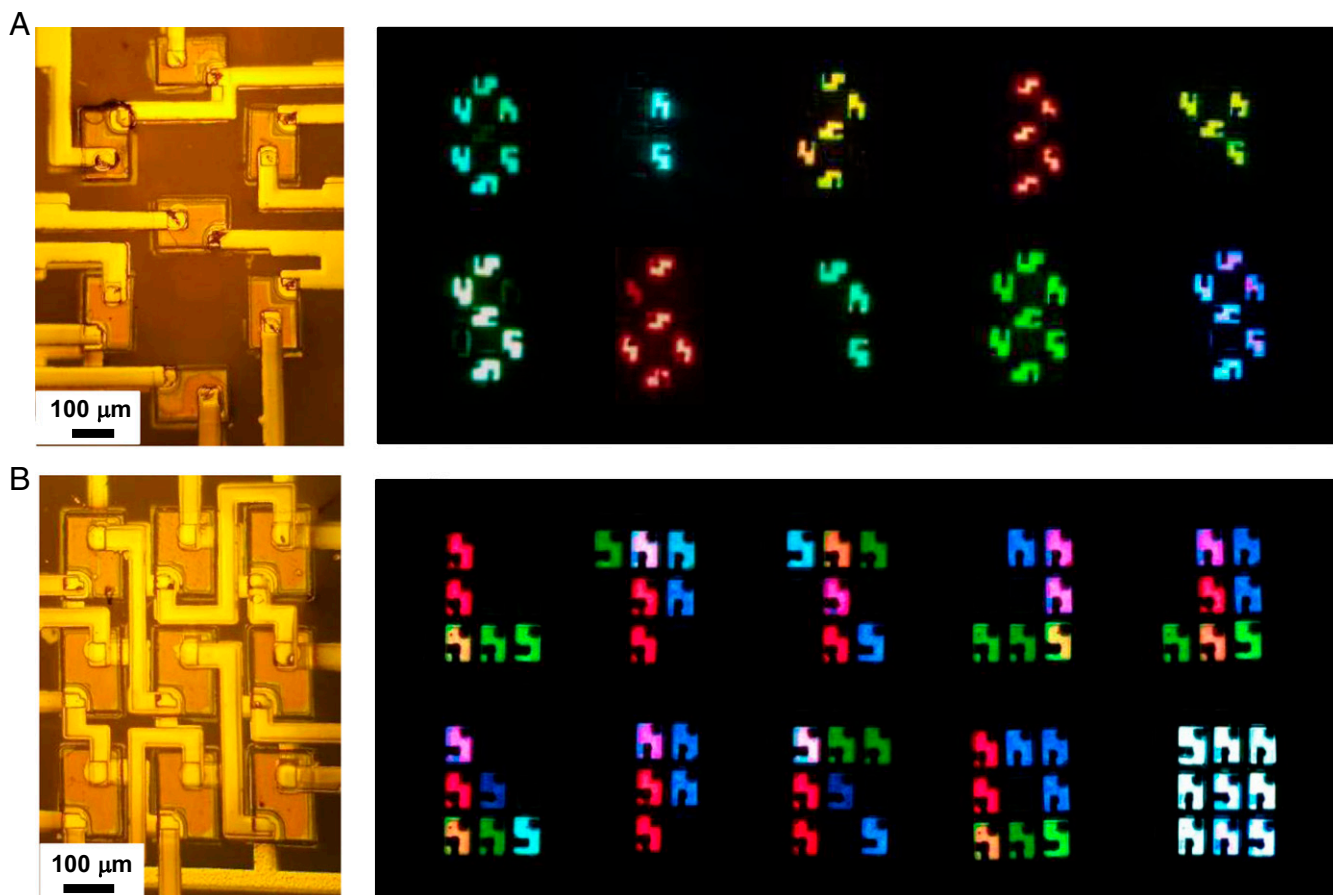
Li et al.
Transfer-printed, tandem microscale light-emitting diodes for full-color displays

PNAS | 3 of 7
https://doi.org/10.1073/pnas.2023436118

Fig. 3. Arrays of tandem RGB micro-LEDs interconnected for display demonstration. (*A*) Micrograph for an array forming seven-segment display (*Left*), showing decimal numerals 0 through 9 with various colors (*Right*). (*B*) Micrograph for a 3 × 3 array (*Left*), showing different color patterns.

(8) and conventional LCDs (10^2 to 10^3 cd/m²) (5). Fig. 4*C* plots measured external quantum efficiency (EQE) spectra for different micro-LEDs. At currents of 1 to 10 mA, EQEs for micro-LEDs in the tandem structure are in the range of 2% to 6%, mostly limited by the inefficient light extraction at the high-index semiconductor and air interfaces. Since the current state-of-the-art EQEs are around 20% to 50% for LEDs in the lighting field, there is still room for improvement in the future research, for example, by introducing photonic structures for better light extraction (44, 45), reducing nonradiative recombination by sidewall passivation (46), facilitating the thermal dissipation with a heat sink (33), etc. Fig. 4*D* shows measured electrical-to-optical frequency responses for these devices, at a current of 3 mA. The 3 dB modulation bandwidths are around 17 MHz, 9 MHz, and 4 MHz for red, green and blue micro-LEDs, respectively. The results indicate that these micro-LEDs present a fast response time (less than 1 μs) superior to LCDs and OLEDs (typically in the order of 1 to 100 kHz).

As previously described, an optical design for wavelength selective transmission/reflection at the interface between the green and the red micro-LEDs is crucial for optimizing the performance of the tandem RGB devices. High-performance optical filters are normally made of multilayer dielectric structures that are deposited on glass (47). Here, we show that thin-film microscale filters can be heterogeneously integrated into the tandem micro-LED structure, with a similar printing-based approach (Fig. 5). The designed filter structure is made of multilayered titanium dioxide (TiO_2) and silicon dioxide (SiO_2) stacks that are deposited on GaAs by sputtering (Fig. 5*A* and *SI Appendix,* Table S4). Freestanding, thin-film filters with geometries similar to RGB micro-LEDs can be formed

by eliminating the GaAs substrate and laser milling (Fig. 5 *B* and *C*), with fabrication details provided in *SI Appendix,* Fig. S5. Angular-dependent transmittance spectra for a filter membrane printed on glass are measured in Fig. 5 *D* and *E*. Experimental results are in good agreement with optical simulations provided in
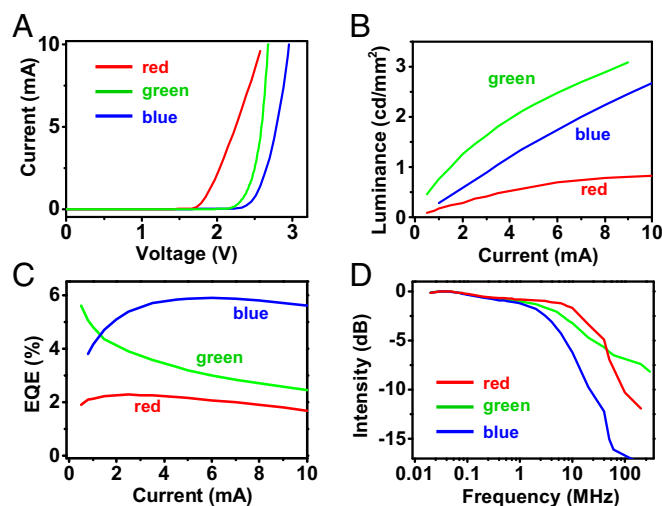

Fig. 4. Optoelectronic properties of the RGB micro-LEDs in a tandem structure. (*A*) Current–voltage curves. (*B*) Brightness versus current. (*C*) EQEs as a function of current. (*D*) Emissive power versus modulation frequency.

Li et al.
Transfer-printed, tandem microscale light-emitting diodes for full-color displays

Table 1. Performance of individual red, green, and blue micro-LEDs in a tandem RGB LED structure

LED color	Red	Green	Blue
λ_{peak} (nm)	628	530	475
Full width at half maxima (FWHM) (nm)	14	32	23
EQE_{max} (%)	2.6	5.8	6.0
η_{max} (cd/A)	4.6	20.6	6.8
V @ η_{max} (V)	1.8	2.3	2.6
V @ 1 cd/mm^2	2.1	2.3	2.6
CIE coordinates (x, y)	(0.68, 0.30)	(0.24, 0.72)	(0.12, 0.14)
3 dB frequency (MHz)	17	9	4

Fig. 5 F and G. At normal incidence, the designed longpass filter exhibit a cutoff wavelength at around 590 nm, achieving >95% transmission at longer wavelengths (red and near infrared) and nearly zero transmission (in other words, ~100% reflection) at shorter wavelengths (green and blue). In the tandem micro-LED structure, the filter layer reflects emissions from the green and the blue micro-LEDs back to the air and permits the transmission of red light. Therefore, the filter design is able to improve the light extraction from the green and the blue micro-LEDs, while maintaining the descent performance for the red micro-LED. Moreover, the filter layer helps minimize the photon coupling among the micro-LEDs. The cutoff wavelength for the filter exhibits a blue shift at oblique angles, which could slightly diminish the efficiencies

of the green micro-LED at emissive angles larger than 40 degrees to normal.

Fig. 6 compares the performance for RGB micro-LEDs in different configurations. Fig. 6A schematically summarizes different device layouts, including RGB micro-LEDs separately printed on polyimide, as well as RGB tandem stacks with and without the filter interlayer. All the micro-LEDs share the same geometries. Fig. 6 B–G plot measured EQEs versus currents as well as far-field angular emission profiles for these micro-LEDs in various structures. For red micro-LEDs, the stacked filter, green, and blue micro-LEDs on top slightly decreases their EQEs (Fig. 6 B and C), because of the intrinsic absorptions in the stacked devices on top, as well as the shadowing effects due
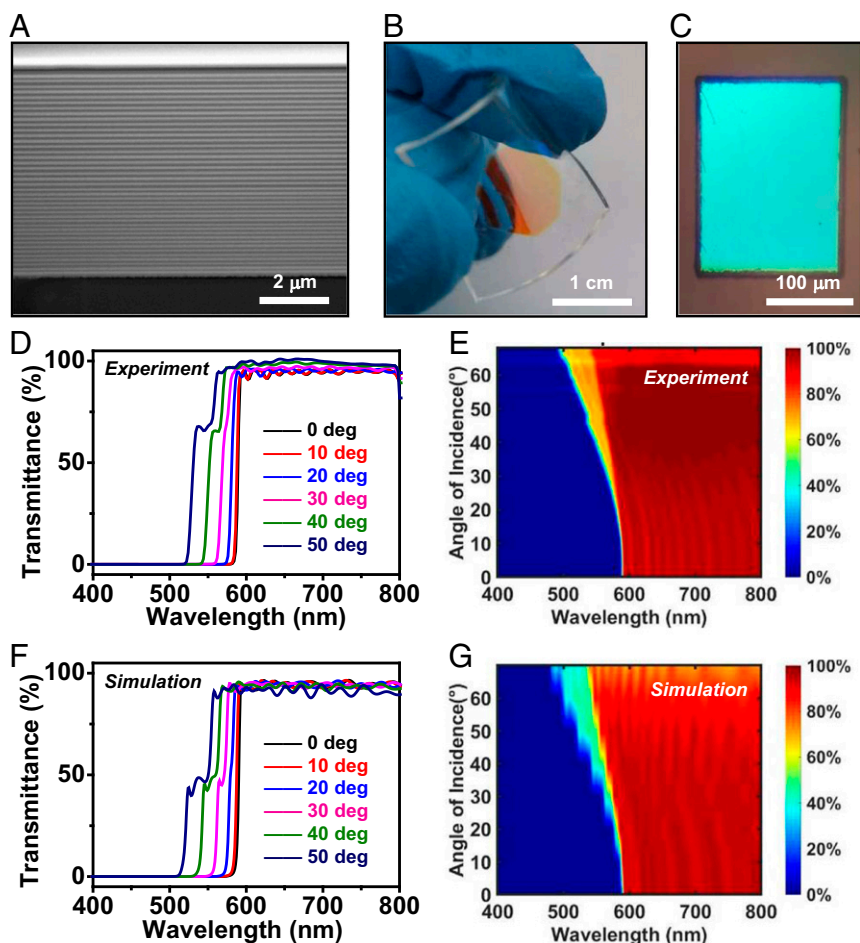

Fig. 5. Structures, images, and optical performance of the thin-film wavelength selective filter. (A) Cross-sectional SEM image showing the multilayered SiO$_2$/TiO$_2$ stacks. (B) Photograph of a released thin-film filter on a flexible polydimethylsiloxane sheet. (C) Microscopic image of a filter (size: 150 μm × 230 μm) patterned by laser milling. (D–G) Measured and simulated transmission spectra and contour plots at varied incident angles for a filter transferred on glass.

Li et al.
Transfer-printed, tandem microscale light-emitting diodes for full-color displays

PNAS | 5 of 7
https://doi.org/10.1073/pnas.2023436118

to the device misalignment. For both green and blue micro-LEDs, the use of the selective filter clearly enhances the emission intensities and device efficiencies (Fig. 6 *D–G*). These micro-LEDs in a tandem structure without filter exhibit lower EQEs than those bare ones due to the strong absorption of the red micro-LED in the bottom. By contrast, the introduction of the filter increases the device efficiencies by more than 50%. All of the micro-LEDs present a near Lambertian radiation pattern, indicating a large viewing angle for desirable display applications.

Conclusion

In this work, we report materials and device assembly strategies to create vertically stacked, tandem inorganic RGB thin-film micro-LEDs and arrays for full-color display demonstrations. The tandem device architecture can mitigate the effects of performance degradation along with the LED size reduction, as well as the stringent quality requirements for fabrication and transfer. Although the micro-LEDs' performances are not optimized and can be further enhanced by using advanced electronic and photonic designs, the inorganic RGB micro-LEDs presented here have already shown full-color coverage, high brightness, and fast response superior to LCDs and OLEDs. The demonstrations here are performed using device with a size of around 125 μm × 180 μm, but these concepts and approaches can be adapted for the assembly of micro-LEDs with sizes of tens of micrometers

and even several micrometers. Unequivocally, challenges remain for manufacturing practice, in terms of massive device transfer to realize large-scale arrays (for example, millions of pixels) with a nearly 100% yield. In addition, the design combining the micro-LED arrays and active driving circuits should be taken into account (42, 48). Compared with conventional lateral RGB configuration, the tandem device design would increase the fabrication complexity and create difficulties for connecting LEDs at different layers with driving circuits. Such challenges can be mitigated by employing planarization and interconnection methods used for standard silicon-based chip fabrication, as well as reducing the LED thicknesses down to the submicrometer scale, which would become necessary for making micro-LEDs smaller than 10 μm for virtual and augmented reality applications. Fast responses of these inorganic micro-LEDs also create possibilities for the integration of telecommunication with lighting and display systems (49). Other potential research directions include employing these tandem micro-LEDs onto flexible, stretchable, and biocompatible substrates for wearable and implantable systems in biomedical areas (50, 51). In summary, these schemes and results establish promising routes to next-generation micro-LED–based lighting and display systems.

Materials and Methods

Device Fabrication. Details about device structures and fabrication process are provided in *SI Appendix*, Figs. S3–S9 and Tables S1–S4. The InGaP-based red
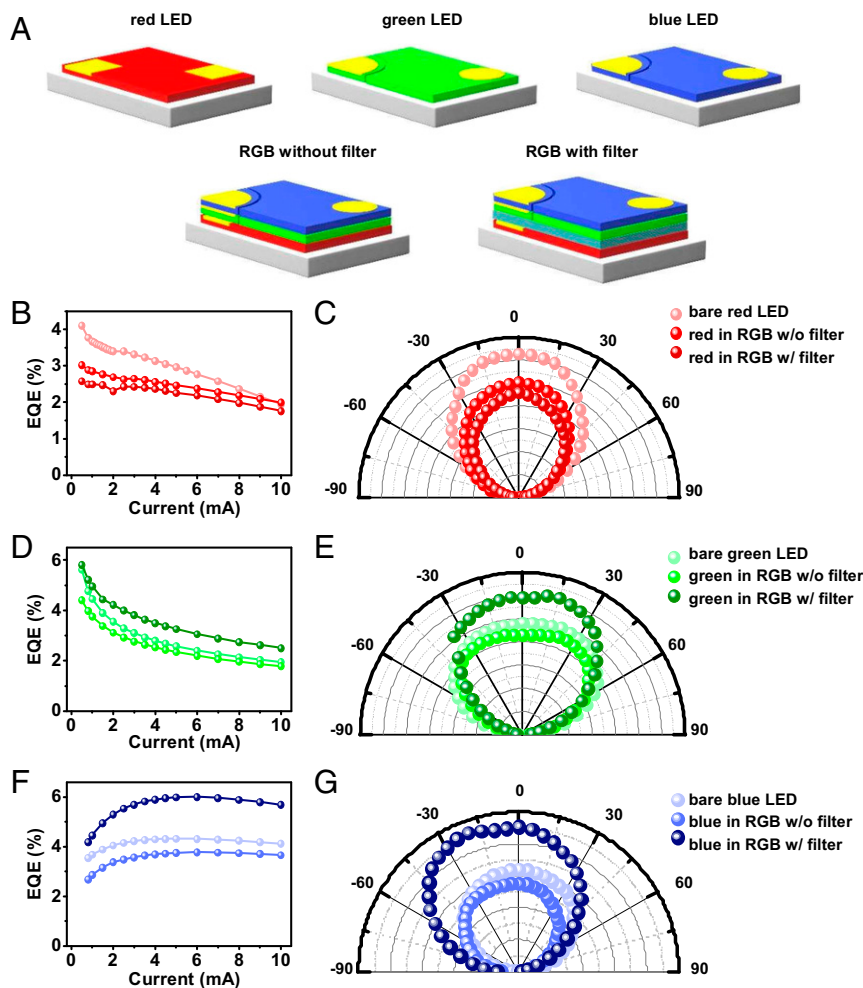

Fig. 6. Schematic illustrations of micro-LEDs on original substrates and those in tandem structures and comparisons of their optical performance. (*A*) Schematic illustrations of individual RGB micro-LEDs (*Top*), and tandem RGB devices with and without the filter interlayer (*Bottom*). (*B–G*) Measured EQEs versus current (*B, D,* and *F*) and angular emission profiles. (*C, E,* and *G*) for bare micro-LEDs and devices in tandem RGB structures. (*B* and *C*) red LEDs; (*D* and *E*) green LEDs; and (*F* and *G*) blue LEDs.

LED structure is grown on a GaAs substrate, and the InGaN-based green and blue LED structures are grown on sapphire, both by metal-organic chemical vapor deposition (MOCVD). The micro-LEDs are fabricated with a standard photolithographic process, and freestanding, thin-film micro-LEDs are formed by selectively etching the $Al_{0.95}Ga_{0.05}As$ sacrificial layer (for red LEDs) (34) or ultraviolet laser liftoff (for green and blue LEDs) (33). The multilayered TiO_2/SiO_2 wavelength selective filter is deposited on GaAs by ion beam–assisted sputtering, with freestanding, thin-film filters formed by wet etching the GaAs and laser milling (35). Tandem device structures comprising RGB micro-LEDs and filters are fabricated by transfer printing with poly(dimethylsiloxane) stamps using a customized setup based on a mask aligner (with a lateral alignment accuracy of less than 5 μm) (32, 39). Spin-coated, thin-film SU-8 epoxy layers serve as bonding interfaces. Sputtered Cr/Au/Cu/Au (10/20/500/60 nm) layers serve as interconnect contacts for different micro-LEDs.

Device Characterization. Current–voltage curves are measured with a Keithley 2400 source meter. LED electroluminescence is measured with a spectrometer (HR2000+, Ocean Optics). EQE is measured using a spectroradiometer system with integrating sphere (LabSphere). SEM images are captured by with an electron microscope (ZEISS Auriga SEM/FIB Crossbeam System, Germany). The optical microscopy images are taken by an optical microscope MC-D800U(C).

The transmittance spectra of the optical filters are measured using an ultraviolet-vis-infrared spectrophotometer (Cary 5000, Varian). For angular dependent emissive profiles, devices are mounted onto a goniometer scanning from −90° to +90° at a step of 5° at an injection current of 3 mA. The emission intensity is captured by a standard Si photodetector (DET36A, Thorlabs). Fluorescence images of the stacked RGB micro-LED array are captured by an Olympus IX53 microscope.

1. H. E. Lee *et al.*, Micro light-emitting diodes for display and flexible biomedical applications. *Adv. Funct. Mater.* **29**, 1808075 (2019).
2. Y. Huang, E.-L. Hsiang, M.-Y. Deng, S.-T. Wu, Mini-LED, micro-LED and OLED displays: Present status and future perspectives. *Light Sci. Appl.* **9**, 105 (2020).
3. H. X. Jiang, J. Y. Lin, Nitride micro-LEDs and beyond—a decade progress review. *Opt. Express* **21**, A475–A484 (2013).
4. T. Wu *et al.*, Mini-LED and micro-LED: Promising candidates for the next generation display technology. *Appl. Sci. (Basel)* **8**, 1557 (2018).
5. D.-K. Yang, S.-T. Wu, *Fundamentals of Liquid Crystal Devices* (John Wiley & Sons, ed. 2, 2015).
6. H.-W. Chen, J.-H. Lee, B.-Y. Lin, S. Chen, S.-T. Wu, Liquid crystal display and organic light-emitting diode display: Present status and future perspectives. *Light Sci. Appl.* **7**, 17168 (2018).
7. J.-H. Lee *et al.*, Blue organic light-emitting diodes: Current status, challenges, and future outlook. *J. Mater. Chem. C* **7**, 5874–5888 (2019).
8. T. Tsujimura, *OLED Display Fundamentals and Applications* (John Wiley & Sons, 2017).
9. H. Zheng *et al.*, All-solution processed polymer light-emitting diode displays. *Nat. Commun.* **4**, 1971 (2013).
10. H. V. Han *et al.*, Resonant-enhanced full-color emission of quantum-dot-based micro LED display technology. *Opt. Express* **23**, 32504–32515 (2015).
11. Y. Jiang, S.-Y. Cho, M. Shim, Light-emitting diodes of colloidal quantum dots and nanorod heterostructures for future emissive displays. *J. Mater. Chem. C* **6**, 2618–2634 (2018).
12. Q. Van Le, H. W. Jang, S. Y. Kim, Recent advances toward high-efficiency halide perovskite light-emitting diodes: Review and perspective. *Small Methods* **2**, 1700419 (2018).
13. S. I. Park *et al.*, Printed assemblies of inorganic light-emitting diodes for deformable and semitransparent displays. *Science* **325**, 977–981 (2009).
14. H. S. Kim *et al.*, Unusual strategies for using indium gallium nitride grown on silicon (111) for solid-state lighting. *Proc. Natl. Acad. Sci. U.S.A.* **108**, 10072–10077 (2011).
15. J. Day *et al.*, III-Nitride full-scale high-resolution microdisplays. *Appl. Phys. Lett.* **99**, 031116 (2011).
16. C. A. Bower *et al.*, Emissive displays with transfer-printed assemblies of 8 μm × 15 μm inorganic light-emitting diodes. *Photon. Res.* **5**, A23–A29 (2017).
17. W. Guo, H. Meng, Y. Chen, T. Sun, Y. Li, Wafer-level monolithic integration of vertical micro-LEDs on glass. *IEEE Photonics Technol. Lett.* **32**, 673–676 (2020).
18. D.-H. K. T.-Y. Seong, Influence of size reduction and current density on the optoelectrical properties of green III-nitride micro-LEDs. *ECS Trans.* **85**, 13–18 (2018).
19. F. Olivier *et al.*, Influence of size-reduction on the performances of GaN-based micro-LEDs for display application. *J. Lumin.* **191**, 112–116 (2017).
20. J. T. Oh *et al.*, Light output performance of red AlGaInP-based light emitting diodes with different chip geometries and structures. *Opt. Express* **26**, 11194–11200 (2018).
21. S. X. Jin, J. Shakya, J. Y. Lin, H. X. Jiang, Size dependence of III-nitride microdisk light-emitting diode characteristics. *Appl. Phys. Lett.* **78**, 3532–3534 (2001).
22. D.-M. Geum *et al.*, Strategy toward the fabrication of ultrahigh-resolution micro-LED displays by bonding-interface-engineered vertical stacking and surface passivation. *Nanoscale* **11**, 23139–23148 (2019).
23. Y. Tchoe *et al.*, Variable-color light-emitting diodes using GaN microdonut arrays. *Adv. Mater.* **26**, 3019–3023 (2014).
24. Y. F. Cheung, H. W. Choi, Color-tunable and phosphor-free white-light multilayered light-emitting diodes. *IEEE Trans. Electron Dev.* **60**, 333–338 (2013).
25. R. Wang *et al.*, Color-tunable, phosphor-free InGaN nanowire light-emitting diode arrays monolithically integrated on silicon. *Opt. Express* **22**, A1768–A1775 (2014).
26. H. S. El-Ghoroury, M. Yeh, J. C. Chen, X. Li, C.-L. Chuang, Growth of monolithic full-color GaN-based LED with intermediate carrier blocking layers. *AIP Adv.* **6**, 075316 (2016).
27. J. Chun *et al.*, Vertically stacked color tunable light-emitting diodes fabricated using wafer bonding and transfer printing. *ACS Appl. Mater. Interfaces* **6**, 19482–19487 (2014).
28. C. M. Kang *et al.*, Vertically-stacked passive-matrix micro-LED array structure for a dual color display. *Opt. Express* **25**, 2489–2495 (2017).
29. K. N. Hui, X. H. Wang, Z. L. Li, P. T. Lai, H. W. Choi, Design of vertically-stacked polychromatic light-emitting diodes. *Opt. Express* **17**, 9873–9878 (2009).
30. M. Fröbel *et al.*, Three-terminal RGB full-color OLED pixels for ultrahigh density displays. *Sci. Rep.* **8**, 9684 (2018).
31. Z. Shen, P. E. Burrows, V. Bulović, S. R. Forrest, M. E. Thompson, Three-color, tunable, organic light-emitting devices. *Science* **276**, 2009–2011 (1997).
32. E. F. Schubert, *Light-Emitting Diodes* (Cambridge University Press, Cambridge, ed. 2, 2006).
33. L. Li *et al.*, Heterogeneous integration of microscale GaN light-emitting diodes and their electrical, optical, and thermal characteristics on flexible substrates. *Adv. Mater. Technol.* **3**, 1700239 (2018).
34. T. I. Kim *et al.*, High-efficiency, microscale GaN light-emitting diodes and their thermal properties on unusual substrates. *Small* **8**, 1643–1649 (2012).
35. H. Ding *et al.*, Microscale optoelectronic infrared-to-visible upconversion devices and their use as injectable light sources. *Proc. Natl. Acad. Sci. U.S.A.* **115**, 6632–6637 (2018).
36. C. Liu *et al.*, High performance, biocompatible dielectric thin-film optical filters integrated with flexible substrates and microscale optoelectronic devices. *Adv. Opt. Mater.* **6**, 1870061 (2018).
37. H. E. Lee *et al.*, Trichogenic photostimulation using monolithic flexible vertical AlGaInP light-emitting diodes. *ACS Nano* **12**, 9587–9595 (2018).
38. M. A. Meitl *et al.*, Transfer printing by kinetic control of adhesion to an elastomeric stamp. *Nat. Mater.* **5**, 33–38 (2005).
39. A. Carlson, A. M. Bowen, Y. Huang, R. G. Nuzzo, J. A. Rogers, Transfer printing techniques for materials assembly and micro/nanodevice fabrication. *Adv. Mater.* **24**, 5284–5318 (2012).
40. S. A. Kazazis, E. Papadomanolaki, Iliopoulos EJIJoP. Polarization-engineered InGaN/GaN solar cells: Realistic expectations for single heterojunctions. *IEEE J. Photovoltaics* **8**, 118–124 (2017).
41. X. Sheng *et al.*, Printing-based assembly of quadruple-junction four-terminal microscale solar cells and their use in high-efficiency modules. *Nat. Mater.* **13**, 593–598 (2014).
42. N. Jain *et al.*, More than microLEDs: Mass transfer of pixel engines for emissive displays. *SID Symposium Digest of Technical Papers* **51**, 642–645 (2020).
43. F. Templier, GaN-based emissive microdisplays: A very promising technology for compact, ultra-high brightness display systems. *J. Soc. Inf. Disp.* **24**, 669–675 (2016).
44. J. J. Wierer, A. David, M. M. Megens, III-nitride photonic-crystal light-emitting diodes with high extraction efficiency. *Nat. Photonics* **3**, 163–169 (2009).
45. X. Sheng *et al.*, Design and fabrication of high-index-contrast self-assembled texture for light extraction enhancement in LEDs. *Opt. Express* **19**, A701–A709 (2011).
46. M. S. Wong *et al.*, High efficiency of III-nitride micro-light-emitting diodes by sidewall passivation using atomic layer deposition. *Opt. Express* **26**, 21324–21331 (2018).
47. H. A. Macleod, *Thin-Film Optical Filters* (CRC Press, 2017).
48. J. J. D. McKendry *et al.*, Visible-light communications using a CMOS-controlled micro-light-emitting-diode array. *J. Lightwave Technol.* **30**, 61–67 (2011).
49. S. Rajbhandari *et al.*, A review of gallium nitride LEDs for multi-gigabit-per-second visible light data communications. *Semicond. Sci. Technol.* **32**, 023001 (2017).
50. H. Xu, L. Yin, C. Liu, X. Sheng, N. Zhao, Recent advances in biointegrated optoelectronic devices. *Adv. Mater.* **30**, e1800156 (2018).
51. Y. Zhao *et al.*, Wirelessly operated, implantable optoelectronic probes for optogenetics in freely moving animals. *IEEE Trans. Electron Dev.* **66**, 785–792 (2018).

ENGINEERING

Li et al.
Transfer-printed, tandem microscale light-emitting diodes for full-color displays

Supporting Information

Theoretical modeling: Performance of micro-LEDs versus device size

In micro-LEDs, the carrier recombination rate R as a function of the carrier density n can be expressed using the ABC model:

$$R = An + Bn^2 + Cn^3 \tag{1}$$

where the coefficients A, B and C represent the Shockley-Read-Hall (SRH) recombination, the radiative recombination, and the Auger recombination, respectively. For most III-V semiconductors, the Auger recombination coefficient (C) is approximately 10^{-30} cm^6 s^{-1}.[1, 2] At low injection currents ($n < 10^{18}$ cm^{-3}) for display purposes, the Auger recombination (Cn^3) can be neglected. At equilibrium, the carrier generation (G) and recombination (R) are balanced. Therefore, the carrier density n is determined by

$$An + Bn^2 = j/{ed} \tag{2}$$

where j is the injected current density (assumed to be 36 A/cm^2 in the following calculations), e is electron charge and d is the thickness of LED active region (j/ed is the carrier generation rate G in the LED). And the internal quantum efficiency η_{int} for radiative emission is simplified as:

$$\eta_{int} = \frac{Bn^2}{An + Bn^2} \tag{3}$$

The SRH recombination is determined by the defects in the bulk material and on the sidewall surface.

$$A = \frac{1}{\tau_{\text{bulk}}} + v_s \frac{1}{L} \tag{4}$$

$1/\tau_{\text{bulk}}$ is the bulk recombination rate, v_s is the surface recombination velocity, and L is the equivalent lateral dimension of the micro-LED (to be specific, the ratio between the volume and sidewall surface area of the LED MQW active region). Combining Eqs. (3) and (4),

$$\eta_{\text{int}} = \frac{Bn^2}{(\frac{1}{\tau_{\text{bulk}}} + v_s \frac{1}{L})n + Bn^2} = \frac{Bn}{\frac{L + v_s \tau_{\text{bulk}}}{L\tau_{\text{bulk}}} + Bn} = \frac{BnL\tau_{\text{bulk}}}{L + v_s \tau_{\text{bulk}} + BnL\tau_{\text{bulk}}} \tag{5}$$

where n is a constant under a fixed current density, and B, τ_{bulk}, v_s are also constants for specific materials. Therefore, η_{int} decreases when the LED size L increases.

For InGaP red LED, B is assumed to be 2×10^{-10} s^{-1} cm^3,[3] τ_{bulk} is approximately 100 ns[4] and v_s is 4×10^4 cm/s.[5] For InGaN blue and green LED, radiative emission parameter B of 1×10^{-8} cm^3 s^{-1} was measured,[6] τ_{bulk} is 10 ns[7] and v_s is 10^4 cm/s.[4] Fig. S1 plots theoretically predicted η_{int} as a function of device sizes for red and blue LEDs. The results are consistent with experimental observations shown in previous studies.[8, 9]

In addition, the tolerance for alignment errors during LED fabrication and transfer assembly also decreases with the device size, as shown in Fig. S2. Here we assume that the tolerance is within +/− 5% of the LED size.[10]

$$\text{tolerance} = \text{LED size} \times 5\%$$

Individual device fabrication

The layout of the stacked RGB micro-LED structure includes (from bottom to top): a polyimide substrate (thickness: 75 μm), an indium gallium phosphide (InGaP) based red LED (size: 140 μm × 195 μm × 7 μm), a SU-8 layer (thickness: 5 μm), an optical filter layer based on multilayer titanium dioxide (TiO_2) and silicon dioxide (SiO_2) (size: 150 μm × 230 μm × 8 μm), a SU-8 layer (thickness: 5 μm), an indium gallium nitride (InGaN) based green LED (size: 125 μm × 180 μm × 7 μm), a SU-8 layer (thickness: 5 μm), an InGaN based blue LED (size: 125 μm × 180 μm × 7 μm). Contacts of each individual LED are metallized with sputtered metal layers (Cr/Au/Cu/Au = 10/100/500/100 nm).

Fabrication of red LEDs

The red LED device structure is grown on a GaAs substrate by metal-organic chemical vapor deposition (MOCVD). The detailed structure is listed in Table S1, which involves (from bottom to top): the GaAs substrate, an $Al_{0.95}Ga_{0.05}As$ sacrificial layer and an $In_{0.5}Ga_{0.5}P$ red LED. Active areas of the InGaP LED (area: 140 μm × 195 μm) are defined by photolithographic process and acid based wet etching. Sputtered metal layers (Ge/Ni/Au for n-GaAs and Cr/Au for p-GaAs) serve as cathode and anode, respectively. After removing the $Al_{0.95}Ga_{0.05}As$ sacrificial layer in a hydrofluoric acid (HF) based solution (HF:water = 1:10 by volume), patterned photoresist works as anchors to tether free-standing thin-film devices on the GaAs substrates. Using poly (dimethylsiloxane) (PDMS) stamps, released devices can be picked up and transferred onto another substrate.

A detailed description of the process to fabricate the freestanding microscale red LED is listed below (also see Fig. S3 and Ref. 11)[11]:

1. Deposit 500 nm thick SiO_2 by PECVD.

2. Clean the wafer with acetone, isopropyl alcohol (IPA), and deinoized (DI) water.

3. Dehydrate at 110 °C for 10 min.

4. Spin coat positive photoresist (PR) (SPR220-v3.0, Microchem, 500 rpm / 5 s, 3000 rpm / 45 s) and soft-bake at 110 °C for 1.5 min.

5. Expose PR with UV lithography tools (URE-2000/25, IOE CAS) with a dose of 300 mJ/cm^2 through a chrome mask and post-bake at 110 °C for 1.5 min.

6. Develop PR in aqueous base developer (AZ300 MIF), rinse with DI water and hard-bake at 110 °C for 20 min.

7. Etch SiO_2 with buffered oxide etchant (BOE 6:1) for ~100 s and rinse with DI water.

8. Clean the PR in processed wafer using acetone, IPA, DI water.

9. Etch GaP in a mixture of KOH / $K_3[Fe(CN)_6]$ / H_2O (1:4:15, by weight) at 80 °C (hot water bath) for 60 s with gently shaking and rinse with DI water.

10. Etch GaP in a mixture of HCl / H_2O (1:5, by volume) for about 2 mins to remove roughness

11. Clean the processed wafer (acetone, IPA, DI water) and dehydrate at 110 °C for 10 min.

12. Pattern PR SPR220-3.0.

13. Etch InAlP / MQWs / InAlP / DBR in a mixture of HCl / H_3PO_4 (1:1, by volume) for 10 s with vigorous shaking, repeat (3~4 times) until the surface is clean and shiny, and then rinse with DI water.

14. Etch n-GaAs in a mixture of H_3PO_4 / H_2O_2 / H_2O (3:1:25, by volume) for 5 min and rinse with DI water.

15. Remove PR (SPR220-v3.0) in processed wafer using acetone, IPA, DI water.

16. Remove the SiO_2 with BOE 6:1 solution for ~2 mins and rinse with DI water.

17. Clean the processed wafer in step 15 (acetone, IPA, DI water) and dehydrate at 110 °C for 10 min.

18. Spin-coat negative photoresist (AZ nLOF 2070, 500 rpm / 5 s, 3000 rpm/ 45 s) and soft-bake at 110 °C for 2 min.

19. Expose with 365 nm optical lithography with for a dose of 45 mJ/cm^2 through a chrome mask and post-exposure bake at 110 °C for 35 s.

20. Develop PR in aqueous base developer (AZ300 MIF) and rinse with DI water.

21. Sputter 20/20/200 nm of Ge / Ni / Au.

22. Lift-off PR in acetone.

23. Rapid temperature annealing (RTA) at 220 °C for 35 s.

24. Clean the processed wafer in step 23 (acetone, IPA, DI water) and dehydrate at 110 °C for 10 min.

25. Spin-coat negative photoresist (AZ nLOF 2070, 500 rpm / 5 s, 3000 rpm / 45 s) and soft-bake at 110 °C for 2 min.

26. Expose with 365 nm optical lithography with for a dose of 45 mJ/cm^2 through a chrome mask and post-exposure bake at 110 °C for 35 s.

27. Develop PR in aqueous base developer (AZ300 MIF) and rinse with DI water.

28. Sputter 20/200 nm of Cr / Au.

29. Lift-off PR in acetone.

30. Clean the processed wafer in step 29 (acetone, IPA, DI water) and dehydrate at 110 °C for 10 min.

31. Pattern PR SPR220-3.0.

32. Etch GaAs in a mixture of H_3PO_4 / H_2O_2 / H_2O (3:1:25, by volume) for 9 min and rinse with DI water.

33. Clean the processed sample with acetone, IPA, and DI water.

34. Pattern PR SPR220-3.0.

35. Etch in diluted HF (49% HF : DI water = 1:10, by volume) to release the devices from growth substrates for 1.2 hour and rinse with DI water.

36. Then the free-standing red LED arrays are formed and ready for picking up.

Fabrication of green and blue micro-LEDs

The InGaN based green and blue LED structures are grown on 2-inch or 4-inch conventional planar sapphire substrates using MOCVD. The main LED structure (from bottom to top) includes: the sapphire substrate, a GaN buffer layer, an n-GaN, an InGaN / GaN multiple-quantum-well (MQW) layer, a p-GaN and an indium tin oxide layer for top contacts. The detailed structures of blue and green LEDs are listed in Tables S2 and S3, respectively. The thickness of the entire epitaxial structure is about 7 μm. LED devices are lithographically fabricated, with Cr/Au layers serving as ohmic contacts. Inductively couple plasma reactive ion etching (ICP-RIE) is used to define the LED mesa (lateral dimension 180 μm × 125 μm). After bonding the fully fabricated LED arrays onto a thermal release tape (TRT) (Nitto Denko Corp.), laser lift-off (LLO) is applied to separate the thin-film LEDs from sapphire substrates by thermally decompose GaN into gallium (Ga) metal and nitrogen gas at the interface. A krypton

fluoride (KrF) excimer laser at 248 nm (Coherent, Inc., CompexPro110) serves as the light source, with a uniform irradiation area of 5 mm × 15 mm. The power density during LLO is optimized to be around 0.6 J/cm^2 for LEDs. After laser irradiation, the micro LEDs are released from sapphire by mild mechanical force at 70 °C (melting point of Ga is 29.7 °C). The Ga residual is removed by immersing the samples into dilute ammonia (1:5 in water) at room temperature for about 30 mins. By heating up to 120 °C, the LEDs are detached from the TRT (the critical release temperature is about 110 °C) and ready for transfer printing by PDMS. The procedures are shown in Fig. S4 and Ref. 12.

Modeling and Fabrication of thin-film filters

Optical filter design is performed based on the transfer matrix method. The designed TiO$_2$ / SiO$_2$ filter structure (19 nm TiO$_2$ / 15 periods of 89 nm SiO$_2$, 52 nm TiO$_2$ / 63 nm SiO$_2$ / 66 nm TiO$_2$ / 22 periods of 73 nm SiO$_2$ + 42.5 nm TiO$_2$ / 154 nm SiO$_2$, total thickness ~6.6 μm, see Table S4) is deposited on GaAs wafers using ion beam-assisted sputter deposition, with substrates heated up to 300 °C (HB-Optical, Shenyang, China). After laser milling (Nd:YVO$_4$ laser, 1064 nm) the filter to form small rectangles (size: 160 μm × 230 μm), the GaAs substrate is fully removed by wet etching (NH$_4$OH : H$_2$O$_2$: H$_2$O = 1:1:2). The released, freestanding micro-filter can be picked up and transferred by PDMS. The procedures are shown in Fig. S5 and Ref. 13.

Preparation of the adhesive solution

The adhesive solution comprises: bisphenol A glycerolate (1 glycerol / phenol) diacrylate, 3-(Trimethoxysilyl) propyl methacrylate, spin-on-glass (SOG 500F, Filmtronics Inc.), 2-Benzyl-2-(dimethylamino)-4'-morpholinobutyrophenone, and anhydrous ethanol. The weight ratio is 200:100:100:9:2000. Stir at room temperature until full mixing. Store the mixed solution in refrigerator (4 °C) for future use. See Ref. 14.

Fabrication of tandem RGB LEDs

A detailed description of the process to fabrication is listed below:

Substrate preparation

1. Cut the polyimide substrate (thickness: 75 μm) into small pieces (size: 22 mm × 22 mm).

2. Laminate the polyimide film onto a PDMS coated glass slide

    a. Degas PDMS (Sylgard 184) 10 : 1 (base: curing agent, by weight).

    b. Spin cast PDMS to a glass slide (cleaned by $NH_4OH : H_2O_2 : H_2O = 1:1:5$, 80 °C, 10 min) at 500 rpm/ 5 s, 3000 rpm/ 45 s to form a PDMS film (thickness: 40~60 μm).

    c. Bake the glass for ~3.5 min at 110 °C.

    d. Laminate the polyimide film onto the PDMS coated glass. Make sure that the polyimide attaches to PDMS tightly without any bubbles).

    e. Bake the sample for 30 mins at 110 °C until PDMS is fully cured.

Transfer red LEDs

3. Clean the polyimide sample by acetone, isopropyl alcohol (IPA) and deionized (DI) water.

4. Spin coat negative photoresist (PR) (AZ nLOF 2070, 500 rpm / 5 s, 3000 rpm / 30 s) and soft-bake at 110 °C for 2 min.

5. Expose with 365 nm optical lithography with a dose of 45 mJ/cm^2 (URE-2000/25, IOE CAS) through a chrome mask and post-exposure bake at 110 °C for 90 s.

6. Develop PR in aqueous base developer (AZ300 MIF) and rinse with DI water.

7. Deposit 30 nm of Cr as the markers by sputtering.

8. Lift-off PR in acetone.

9. Clean the substrate and dehydrate at 110 °C for 10 min.

10. Spin coat the prepared adhesive liquid (3000 rpm, 45 s) on the substrate and soft-bake at 110 °C for 4 min.

11. Transfer print red LEDs from the source wafer onto the processed substrate with PDMS stamps.

12. Cure under to UV for 1 h and bake at 110 °C for 1 h.

13. Photoresist (SPR220-v3.0 on the device) clean by reactive ion etching with reactive ion etching (O_2, 100 sccm, 90 mTorr, 150 W) for 12 min.

red LED encapsulation

14. Clean the processed wafer in step 13 (acetone, IPA, DI water) and dehydrate at 110 °C for 10 min.

15. Expose to ultraviolet induced ozone (UV Ozone) for 10 min.

16. Spin coat SU8-2002 epoxy (500 rpm / 5 s, 3000 rpm / 30 s).

17. Soft-bake at 65 °C for 1 min and 95 °C for 1 min.

18. Pattern SU-8 to expose contact pads of LED by exposing with UV lithography with a dose of 100 mJ/cm^2.

19. Post-bake at 65 °C for 1 min and 95 °C for 2 min.

20. Develop in propylene glycol monomethyl ether acetate (PGMEA) for 1 min and rinse with IPA.

21. Hard bake at 110 °C for 20 min.

red LED metallization

22. Clean the processed wafer in step 23 (acetone, IPA, DI water) and dehydrate at 110 °C for 10 min.

23. Pattern PR AZ nLOF 2070.

24. Deposit 10 nm / 600 nm / 200 nm of Cr / Cu / Au by sputter coater.

25. Lift-off PR in acetone.

Transfer filters

26. Clean the processed sample in step 25 (acetone, IPA, DI water) and dehydrate at 110 °C for 10 min.

27. Expose to ultraviolet induced ozone (UV Ozone) for 10 min.

28. Spin coat SU8-3005 epoxy (500 rpm / 5 s, 3000 rpm / 30 s).

29. Soft-bake at 65 °C for 30 s.

30. Transfer print filters on top of red LEDs with PDMS stamps.

31. Pattern epoxy by exposing with UV lithography tools with a dose of 150 mJ/cm^2.

32. Post-bake at 65 °C for 1 min and 95 °C for 3 min.

33. Develop the exposed area in propylene glycol monomethyl ether acetate (PGMEA) for 1 min and rinse with IPA.

34. Hard-bake at 110 °C for 20 min.

Transfer green LEDs

35. Clean the processed sample in step 34 (acetone, IPA, DI water) and dehydrate at 110 °C for 10 min.

36. Expose to ultraviolet induced ozone (UV Ozone) for 10 min.

37. Spin coat SU8-3005 epoxy (500 rpm / 5 s, 3000 rpm / 30 s).

38. Soft-bake at 65 °C for 30 s.

39. Transfer print green LEDs on top of red LEDs with PDMS stamps.

40. Pattern epoxy by exposing with UV lithography tools with a dose of 150 mJ/cm^2.

41. Post-bake at 65 °C for 1 min and 95 °C for 3 min.

42. Develop the exposed area in propylene glycol monomethyl ether acetate (PGMEA) for 1 min and rinse with IPA.

43. Hard-bake at 110 °C for 20 min.

Green LED metallization

44. Clean the processed sample in step 43 (acetone, IPA, DI water) and dehydrate at 110 °C for 10 min.

45. Expose to ultraviolet induced ozone (UV Ozone) for 10 min.

46. Spin coat SU8-3005 (500 rpm / 5 s, 3000 rpm / 30 s).

47. Soft-bake at 65 °C for 1 min and 95 °C for 3 min.

48. Pattern SU-8 to expose contact pads of LEDs by exposing with UV lithography with a dose of 150 mJ/cm^2.

49. Post-bake at 65 °C for 1 min and 95 °C for 3 min.

50. Develop in propylene glycol monomethyl ether acetate (PGMEA) for 1 min and rinse with IPA.

51. Hard bake at 110 °C for 20 min.

52. Clean the processed wafer in step 51 (acetone, IPA, DI water) and dehydrate at 110 °C for 10 min.

53. Pattern PR AZ nLOF 2070.

54. Roughen surface by reactive ion etching (O_2, 100 sccm, 90 mTorr, 150 W) for 10s.

55. Deposit 10 nm / 600 nm / 200 nm of Cr / Cu / Au by sputtering.

56. Lift-off PR in acetone.

Transfer blue LEDs

57. Clean the processed sample in step 56 (acetone, IPA, DI water) and dehydrate at 110 °C for 10 min.

58. Expose to ultraviolet induced ozone (UV Ozone) for 10 min.

59. Spin coat SU8-3005 epoxy (500 rpm / 5 s, 3000 rpm / 30 s).

60. Soft-bake at 65 °C for 30 s.

61. Transfer printing blue LEDs on top of green LEDs with PDMS stamps.

62. Pattern epoxy by exposing with UV lithography tools with a dose of 150 mJ/cm^2.

63. Post-bake at 65 °C for 1 min and 95 °C for 3 min.

64. Develop the exposed area in propylene glycol monomethyl ether acetate (PGMEA) for 1 min and rinse with IPA.

65. Hard-bake at 110 °C for 20 min.

Blue LED metallization

66. Clean the processed sample in step 65 (acetone, IPA, DI water) and dehydrate at 110 °C

for 10 min.

67. Expose to ultraviolet induced ozone (UV Ozone) for 10 min.

68. Spin coat SU8-3005 (500 rpm / 5 s, 2000 rpm / 30 s).

69. Soft-bake at 65 °C for 1 min and 95 °C for 3 min.

70. Pattern SU-8 to expose contact pads of LEDs by UV lithography with a dose of 150 mJ/cm^2.

71. Post-bake at 65 °C for 1 min and 95 °C for 3 min.

72. Develop in propylene glycol monomethyl ether acetate (PGMEA) for 1 min and rinse with IPA.

73. Hard bake at 110 °C for 20 min.

74. Clean the processed sample in step 73 (acetone, IPA, DI water) and dehydrate at 110 °C for 10 min.

75. Pattern PR AZ nLOF 2070.

76. Roughen surface by reactive ion etching (O$_2$, 100 sccm, 90 mTorr, 150 W) for 10s.

77. Deposit 10 nm / 600 nm / 200 nm of Cr / Cu / Au by sputtering.

78. Lift-off PR in acetone.

Device encapsulation and laser milling

79. Clean the processed sample in step 78 (acetone, IPA, DI water) and dehydrate at 110 °C for 10 min.

80. Expose to ultraviolet induced ozone (UVO) for 10 min.

81. Pattern SU8-3005 epoxy (500 rpm / 5 s, 3000 rpm / 30 s), cure under to UV for 150 mJ / cm^2 and bake at 100 °C for 30 min.

Device characterization

Current–voltage characteristics of micro-LEDs are recorded using a computer-controlled Keithley 2400 source meter. LED electroluminescence is measured with a spectrometer (HR2000+, Ocean Optics). EQE is measured using a spectroradiometer system with integrating sphere (LabSphere). For frequency response measurement, LEDs are modulated at different frequencies (0.001–100 MHz) by a function generator. The light is detected with a silicon detector (Thorlabs, PAD 10), and the signals are transferred to an oscilloscope (Tektronix, DSA 71254C). The FIB-SEM image is captured by with an electron microscope (ZEISS Auriga SEM / FIB Crossbeam System, Germany). The optical microscopy images are taken by a optical microscope MC-D800U(C). The transmittance spectra of the optical filters are measured using a UV-vis-IR spectrophotometer (Cary 5000, Varian). Typical scans are performed from 400 nm to 800 nm with a 2 nm resolution at every 5° from 0° to 70°. For angular dependent emissive profiles, devices are mounted onto a goniometer scanning from −90° to 90° at a step of 5°, at an injection current of 3 mA. The emission intensity is captured by a standard Si photodetector (DET36A, Thorlabs). Fluorescence images of the stacked RGB micro-LED array are captured by an Olympus IX53 microscope equipped with a Xenon arc lamp, in which the excitation light and the emission light pass through a set of fluorescence filter combinations (red: EX AT540/25×, BS AT565DC, EM AT605/55m; green: EX AT480/30×, BS AT505DC, EM AT535/40m; blue: EX AT375/28×, BS AT415DC, EM AT460/50m; Chroma Tech. Corp.).

LED luminance and current efficiency

The luminous flux of micro-LEDs, Φ_{lum}, is obtained from the radiometric light power using the equation

$$\Phi_{lum} = 683 \frac{lm}{W} \int_{\lambda} V(\lambda) P(\lambda) d\lambda \tag{6}$$

where $P(\lambda)$ is the power spectral density measured by the integrating sphere (LabSphere), i.e. the light power emitted per unit wavelength, and the refactor 683 lm/W is a normalization factor. $V(\lambda)$ is the conversion between radiometric and photometric units, which is provided by the luminous efficiency function or eye sensitivity function. This function is referred to the *CIE 1931 V(λ) function*.

Luminance is the luminous flux per steradian (sr) per chip (here we assume our micro-LEDs have an ideal Lambertian emission profile):

$$\text{Luminance} = \frac{\Phi_{lum}}{sr \times area} = 683 \times \pi \times \frac{lm}{W \times area} \int_{\lambda} V(\lambda) P(\lambda) d\lambda \tag{7}$$

$$CE = \frac{\Phi_{lum}}{sr \times I} = 683 \times \pi \times \frac{lm}{W \times I} \int_{\lambda} V(\lambda) P(\lambda) d\lambda \tag{8}$$

For a given power-spectral density $P(\lambda)$, the degree of stimulation required to match the color of $P(\lambda)$ is given by

$$X = \int_{\lambda} \bar{x}(\lambda) P(\lambda) d\lambda \tag{9}$$

$$Y = \int_{\lambda} \bar{y}(\lambda) P(\lambda) d\lambda \tag{10}$$

$$Z = \int_{\lambda} \bar{z}(\lambda) P(\lambda) d\lambda \tag{11}$$

The chromaticity coordinates x and y are calculated from the tristimulus values according to

$$x = \frac{X}{X + Y + Z} \tag{12}$$

$$y = \frac{Y}{X+Y+Z}$$

$$(13)$$

Thus, the value of a chromaticity coordinate is the stimulation of each primary light (or of each type of retinal cone) divided by the entire stimulation $(X + Y + Z)$[15].

References

1.   Ferrini R, Guizzetti G, Patrini M, Parisini A, Tarricone L, Valenti B. Optical functions of InGaP/GaAs epitaxial layers from 0.01 to 5.5 eV. The European Physical Journal B - Condensed Matter 2002, 27(4): 449-458.

2.   Zhang M, Bhattacharya P, Singh J, Hinckley J. Direct measurement of auger recombination in $In_{0.1}Ga_{0.9}N/GaN$ quantum wells and its impact on the efficiency of $In_{0.1}Ga_{0.9}N/GaN$ multiple quantum well light emitting diodes. Applied Physics Letters 2009, 95(20).

3.   Walker AW, Schon J, Dimroth F. Extracting Nonradiative Parameters in III–V Semiconductors Using Double Heterostructures on Active p-n Junctions. IEEE Journal of Photovoltaics 2018, 8(2): 633-639.

4.   Boroditsky M, Gontijo I, Jackson M, Vrijen R, Yablonovitch E, Krauss TF, et al. Surface Recombination Measurements on III-V Candidate Materials for Nanostructure Light-Emitting Diodes. Journal of Applied Physics 2000, 87(7): 3497-3504.

5.   Pearton SJ. Comparison of surface recombination velocities in InGaP and AlGaAs mesa diodes. Journal of Vacuum Science & Technology B 1994, 12(1).

6.   Muth JF, Lee JH, Shmagin IK, Kolbas RM, Casey HC, Keller BP, et al. Absorption coefficient, energy gap, exciton binding energy, and recombination lifetime of GaN obtained from transmission measurements. Applied Physics Letters 1997, 71(18): 2572-2574.

7.   Hu Z, Nomoto K, Song B, Zhu M, Qi M, Pan M, et al. Near unity ideality factor and Shockley-Read-Hall lifetime in GaN-on-GaN p-n diodes with avalanche breakdown. Applied Physics Letters 2015, 107(24): 243501.

8.   Oh J, Lee S, Moon Y, Moon JH, Park S, Hong KY, et al. Light output performance of red AlGaInP-based light emitting diodes with different chip geometries and structures. Optics Express 2018, 26(9): 11194-11200.

9.   Olivier F, Tirano S, Dupre L, Aventurier B, Largeron C, Templier F. Influence of size-reduction on the performances of GaN-based micro-LEDs for display application. Journal of Luminescence 2017, 191: 112-116.

10.   Geum D-M, Kim SK, Kang C-M, Moon S-H, Kyhm J, Han J, et al. Strategy toward the fabrication of ultrahigh-resolution micro-LED displays by bonding-interface-engineered vertical stacking and surface passivation. Nanoscale 2019, 11(48): 23139-23148.

11.   Ding H, Lu L, Shi Z, Wang D, Li L, Li X, et al. Microscale optoelectronic infrared-to-visible upconversion devices and their use as injectable light sources. Proceedings of the National Academy of Sciences 2018, 115(26): 6632-6637.

12.   Li L, Liu C, Su Y, Bai J, Wu J, Han Y, et al. Heterogeneous Integration of Microscale GaN Light-Emitting Diodes and Their Electrical, Optical, and Thermal Characteristics on Flexible Substrates. Advanced Materials Technologies 2018, 3(1): 1700239.

13.   Liu C, Zhang Q, Wang D, Zhao G, Cai X, Li L, et al. High Performance, Biocompatible Dielectric Thin-Film Optical Filters Integrated with Flexible Substrates and Microscale Optoelectronic Devices. Advanced Optical Materials 2018, 6(15).

14.   Kim T-i, Kim MJ, Jung YH, Jang H, Dagdeviren C, Pao HA, et al. Thin Film Receiver Materials for Deterministic Assembly by Transfer Printing. Chemistry of Materials 2014, 26(11): 3502-3507.

15.   Schubert, E. Fred, Thomas Gessmann, and Jong Kyu Kim. Light emitting diodes. Kirk-Othmer Encyclopedia of Chemical Technology (2000).

Figure S1
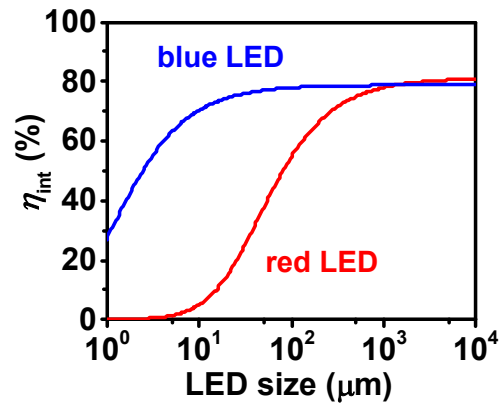
Figure S1. Theoretically modeled performance (internal quantum efficiencies) for an InGaN based blue LED and an InGaP based red LED, as a function of the LED size. Here we assume both LEDs have a square shape.

Figure S2
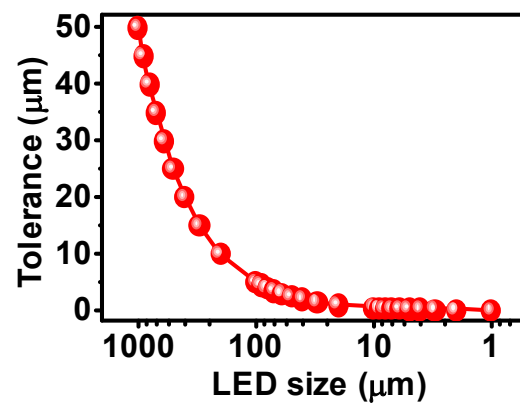
Figure S2. Estimated alignment tolerance for errors during LED microfabrication and transfer printing, as a function of the LED size. Here the tolerance is assumed to be within +/− 5% of the LED size.

Figure S3

epi-structure

lithographic
fabrication

Red LEDs

photoresist
anchoring

Sacrificial layer
wet etching

GaAs

Epi-grown wafer

micro-LEDs on wafer

pick up with
PDMS stamps

PDMS stamps

transfer printing

micro-LEDs on target substrates

micro-LEDs on PDMS
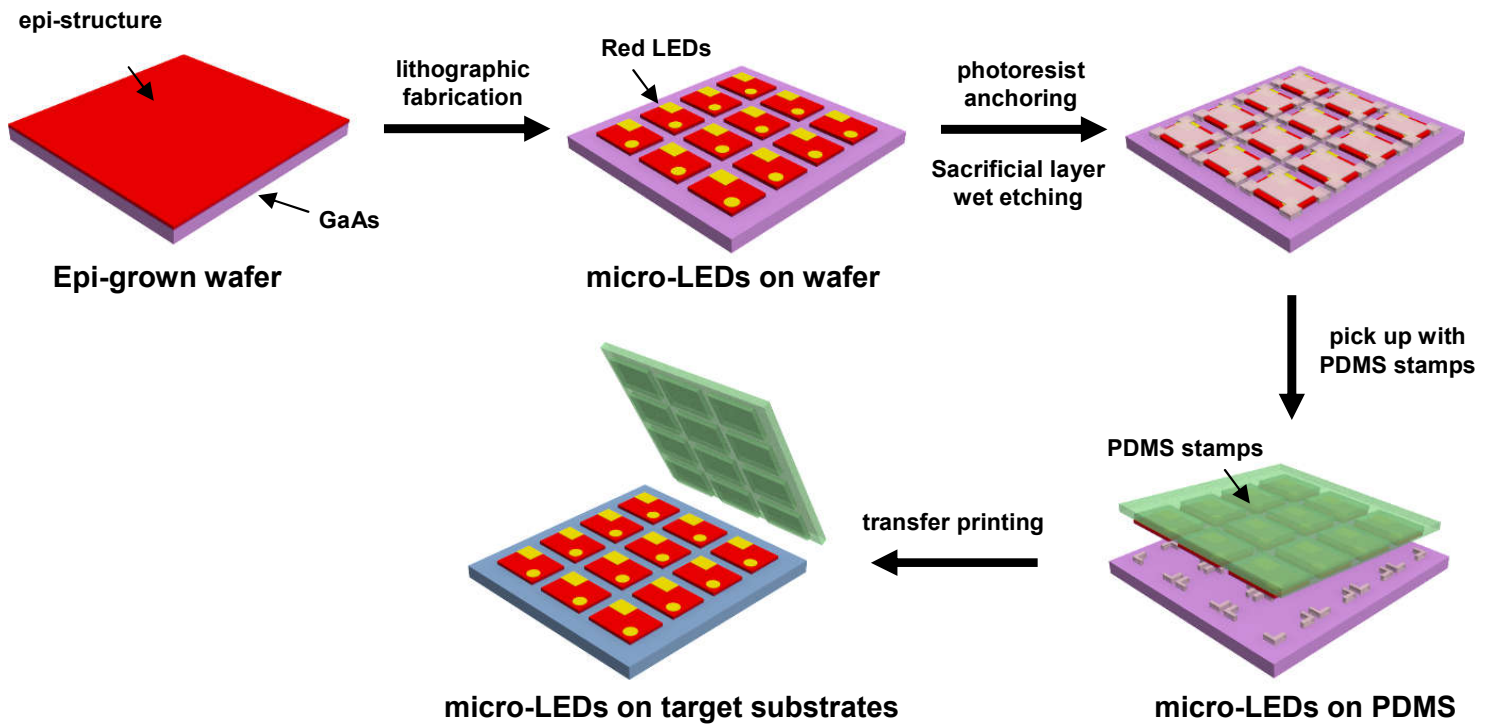
Figure S3. Schematic illustration of the process flow for fabricating and transfer printing InGaP based red LEDs, including epitaxial growth, lithographic fabrication, sacrificial layer etching, PDMS pick up and transfer printing.

Figure S4
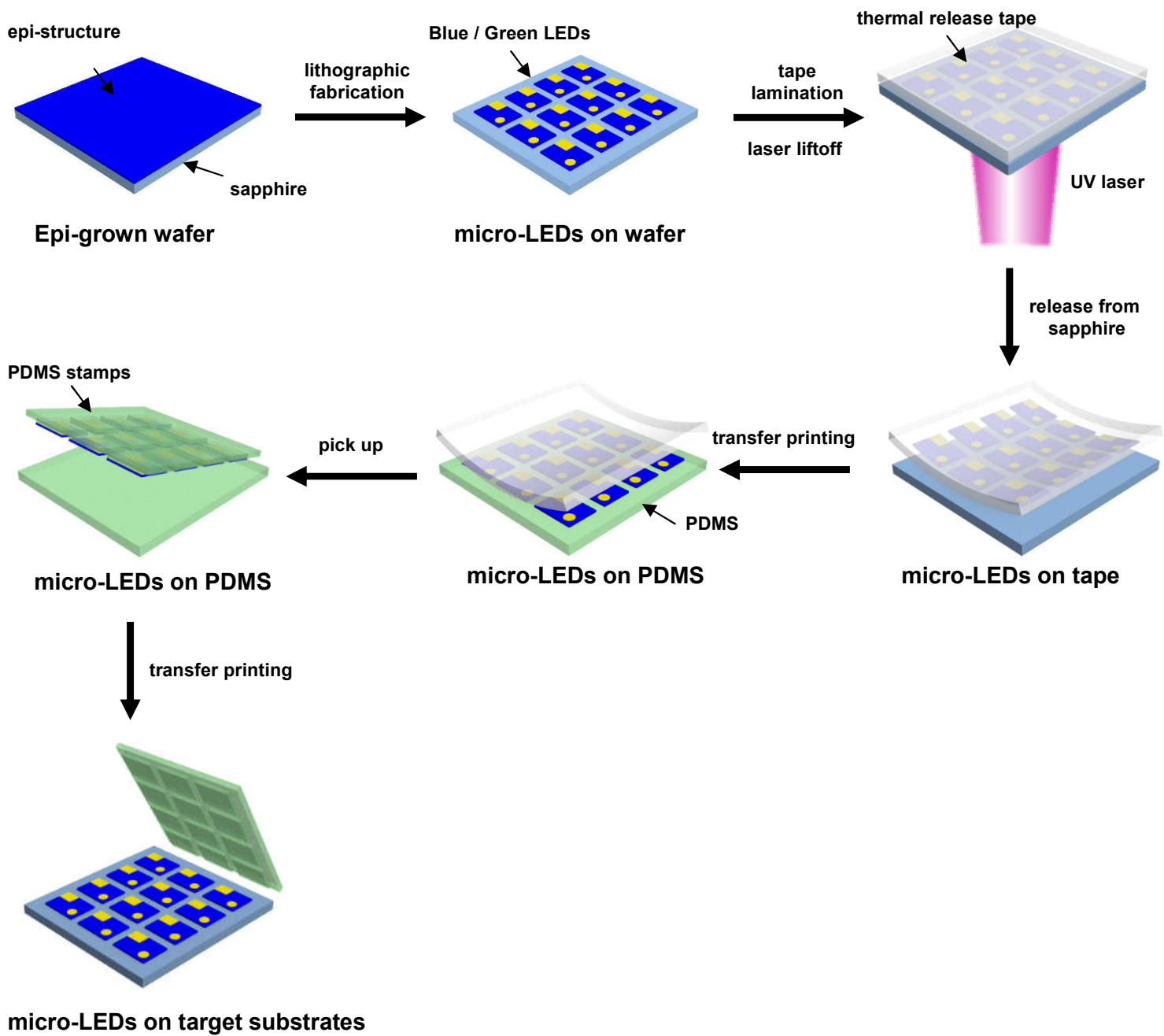
Figure S4. Schematic illustration of the process flow for fabricating and transfer printing InGaN based blue and green LEDs, including epitaxial growth, lithographic fabrication, laser lift-off, thermal release tape release, PDMS pick up and transfer printing.

Figure S5
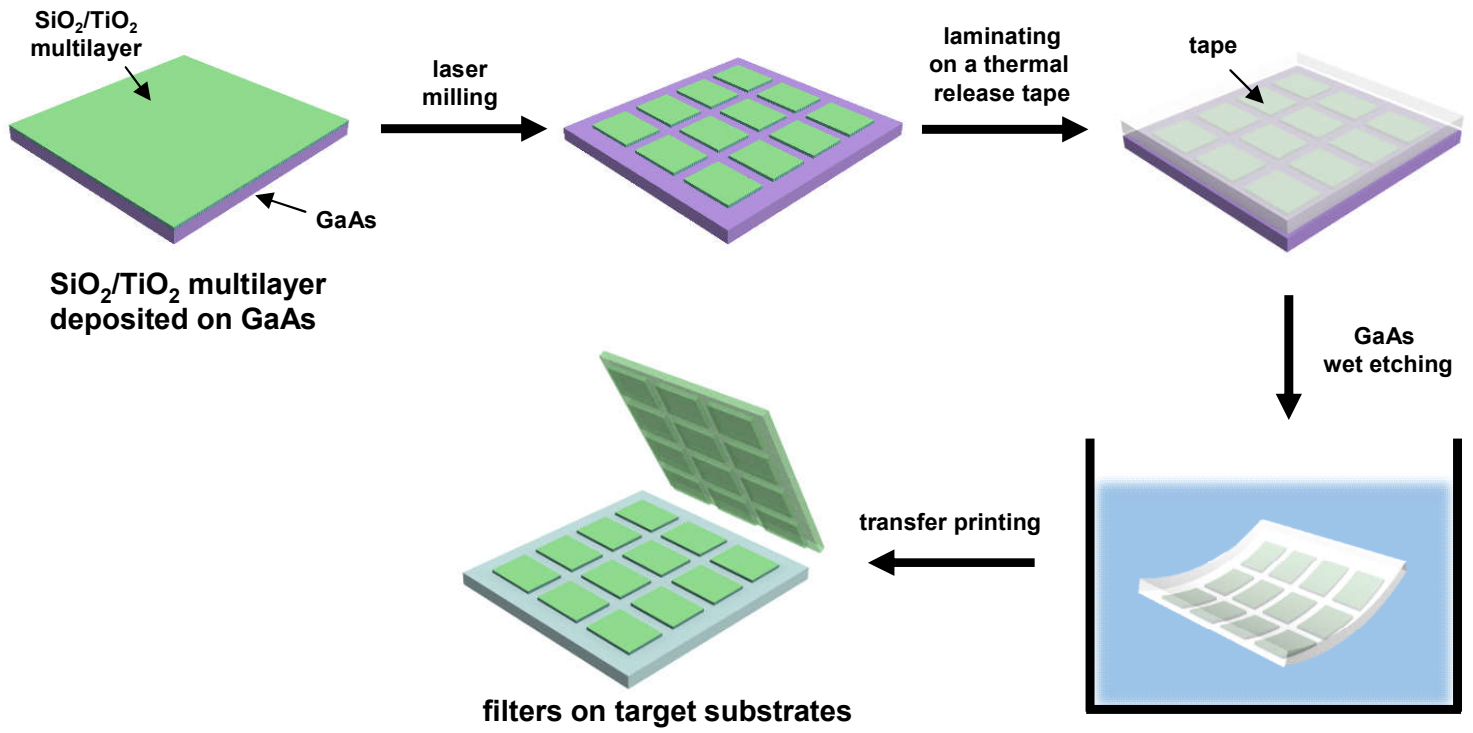
Figure S5. Schematic illustration of the process flow for fabricating and transfer printing SiO$_2$/TiO$_2$ based multilayered optical filters, including oxide deposition, laser milling, GaAs substrate etching and transfer printing.

Figure S6
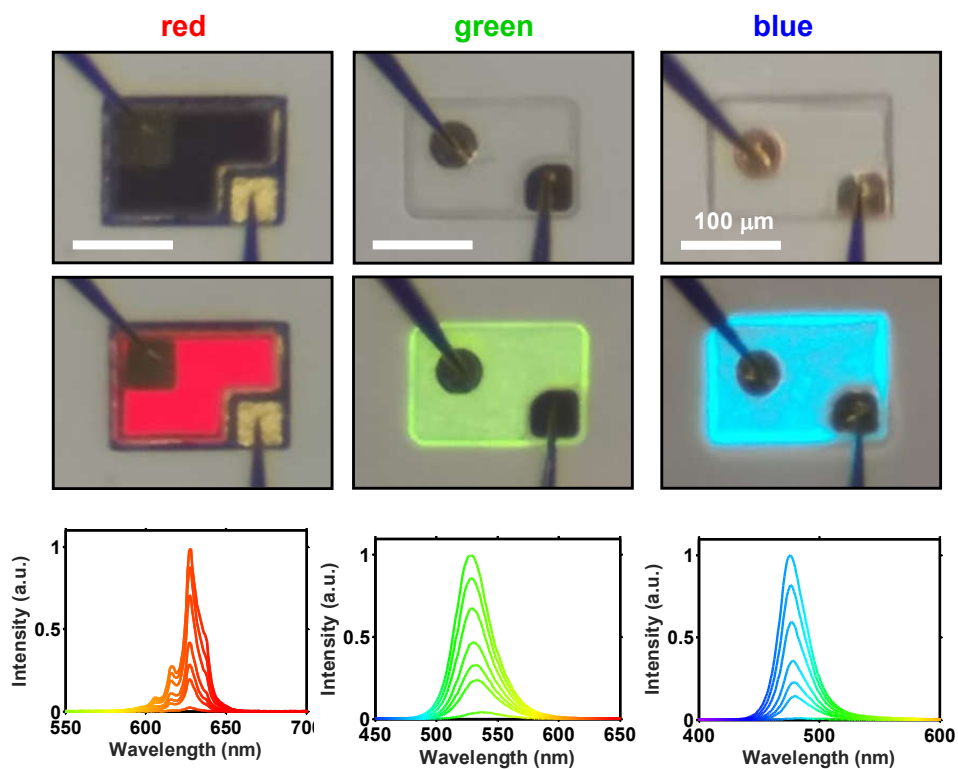
Figure S6. Microscope images of individual red (right), green (middle) and blue (right) micro-LEDs with (top) and without (middle) electroluminescence, and their corresponding electroluminescence spectra with varied injected currents.

Figure S7
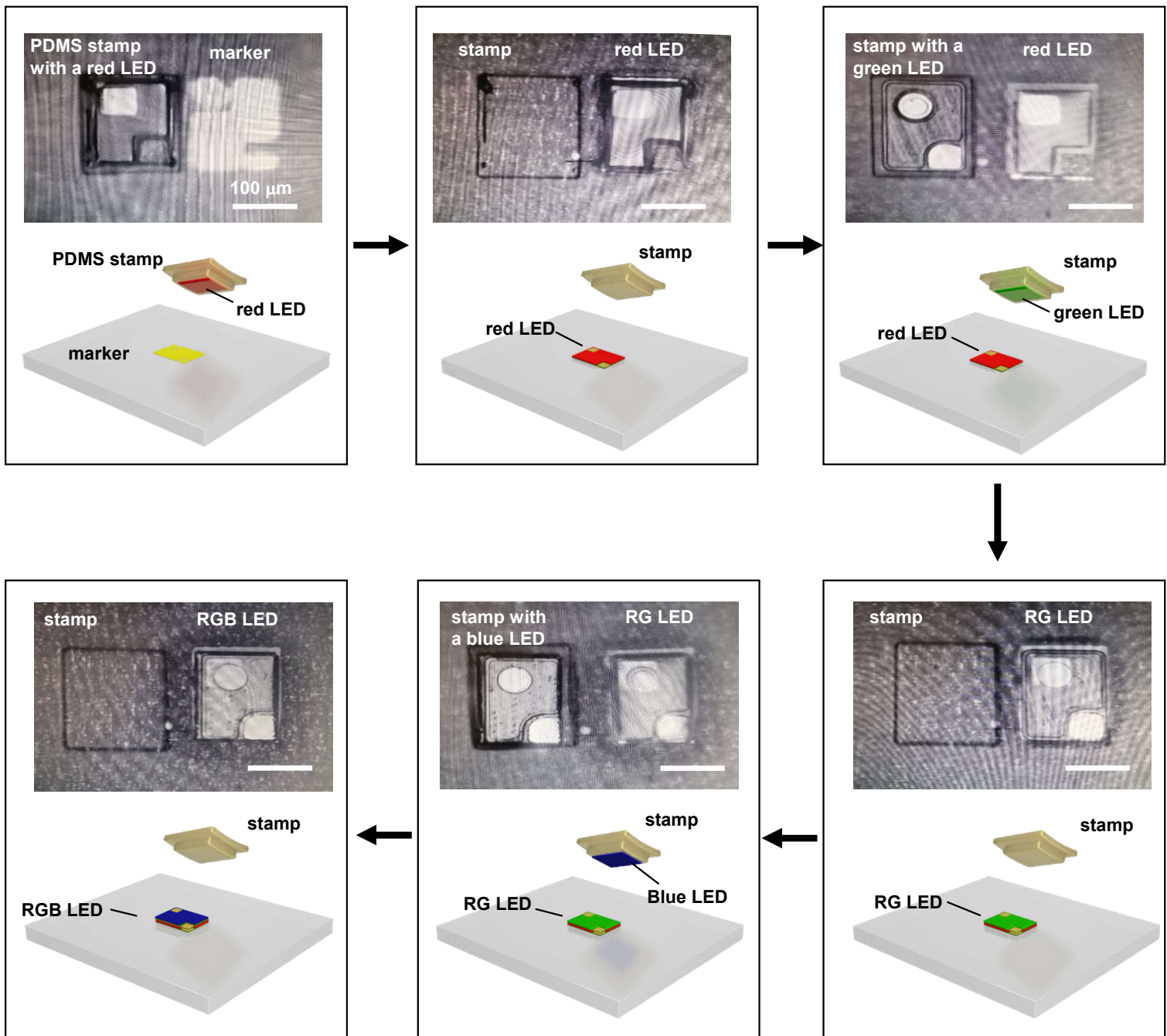
Figure S7. Microscope images and corresponding schematic illustration of the process flow for fabricating a tandem RGB micro-LEDs structure by transfer printing, here the transfer process of the thin-film filter layer is not included, in order to display the LED structures.

Figure S8
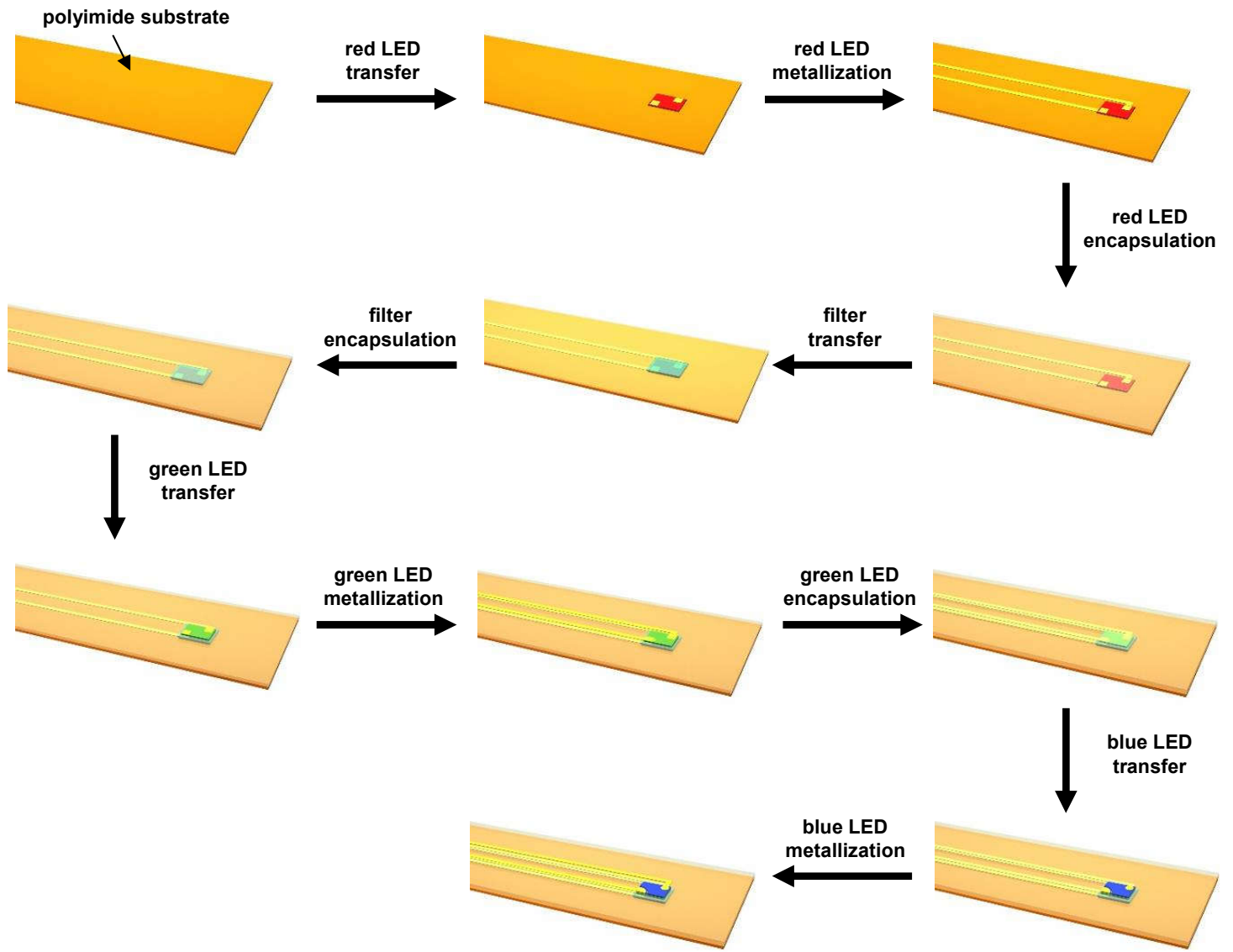
Figure S8. Schematic illustration of the process flow for fabricating the tandem RGB micro-LEDs.
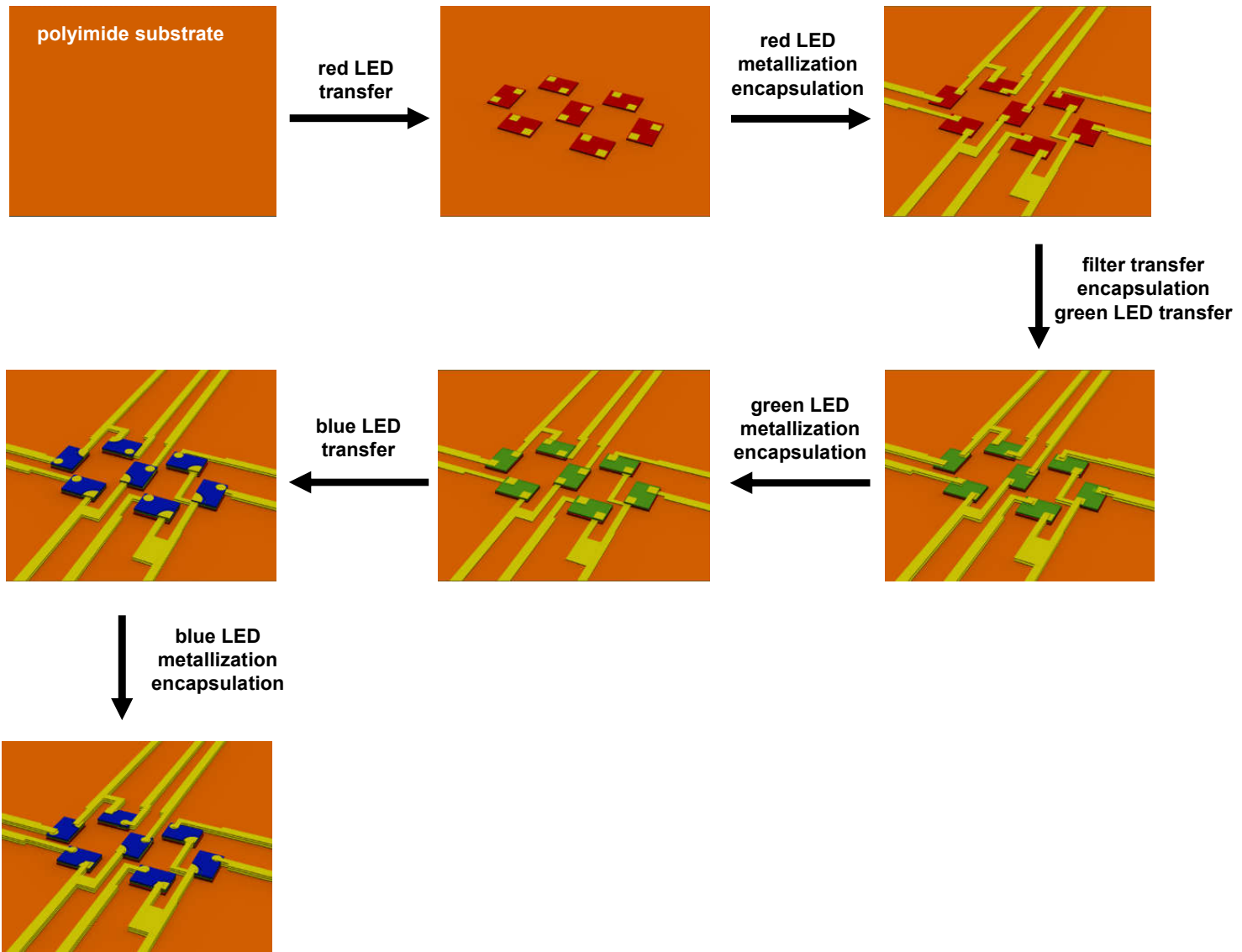
Figure S9

polyimide substrate

red LED transfer

red LED metallization encapsulation

filter transfer encapsulation green LED transfer

green LED metallization encapsulation

blue LED transfer

blue LED metallization encapsulation

Figure S9. Schematic illustration of the process flow for fabricating an array of tandem RGB micro-LEDs.

Figure S10
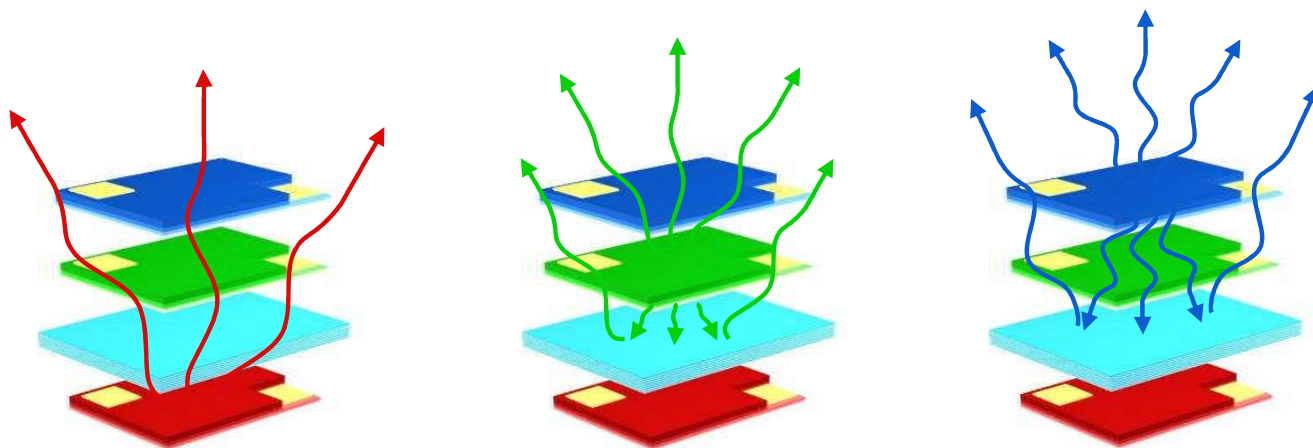
Figure S10. Schematic illustration of the irradiation from the red, green and blue micro-LEDs in a tandem stack with a thin-film filter.
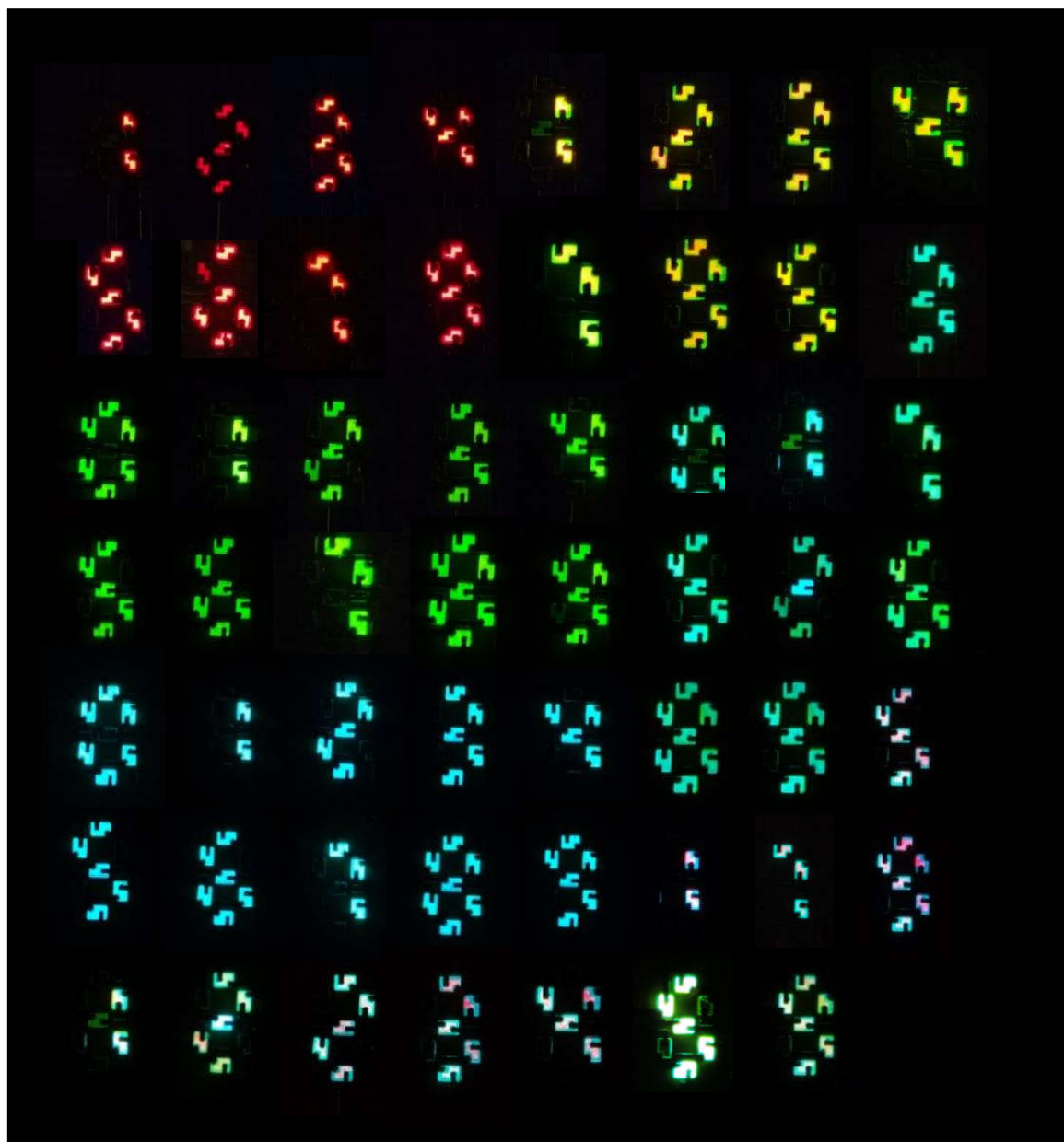
Figure S11

Figure S11. Images of various decimal numerals shown by an array of tandem RGB micro-LEDs forming a seven-segmented display.
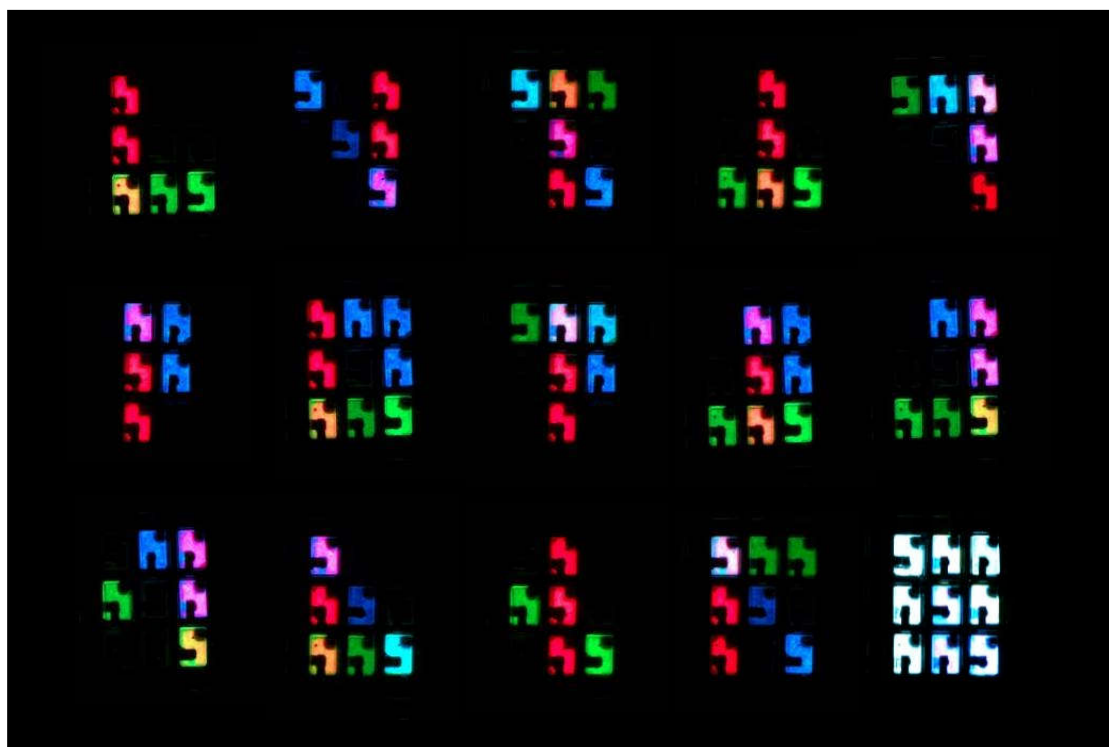
Figure S12

Figure S12. Images of different patterns displayed with a 3*3 array of tandem RGB micro-LEDs.

Table S1

materials	thickness (nm)	doping (cm^{-3})	dopant
p++ GaP contact	200	1e20	C
p+ GaP window	2000	5e18	Mg
p InAlP	800	1e18	Mg
InAlP / InGaP MQWs	200	-	-
n InAlP	200	8e17	Si
In$_{0.5}$Al$_{0.5}$P / In$_{0.5}$Al$_{0.25}$Ga$_{0.25}$P reflector 12 loops	1200	3e18	Si
n+ GaAs contact	1000	6e18	Si
Al$_{0.95}$Ga$_{0.05}$As sacrificial	500	-	-
GaAs substrate	-	-	-

Table S1. Epitaxial structure of the InGaP red LED wafer. The arrow indicates the light emission direction for the red LED, which is unidirectional because of the In$_{0.5}$Al$_{0.5}$P / In$_{0.5}$Al$_{0.25}$Ga$_{0.25}$P multilayered reflector underneath the InAlP / InGaP MQWs.

Table S2

materials	thickness (nm)
ITO	230
p+ GaN	120
Electron blocking layer	20
MQWs	130
Strained layers	300
n+ GaN	3000
u GaN	3500
sapphire substrate	-

Table S2. Epitaxial structure of the InGaN blue LED wafer. The arrow indicates the light emission direction for the blue LED, which is bidirectional.

Table S3

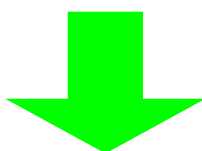| materials	thickness (nm)
ITO	230
p+ GaN + MQWs	800
n+ GaN	2100
u GaN	4000
sapphire substrate	-

Table S3. Epitaxial structure of the InGaN green LED wafer. The arrow indicates the light emission direction for the green LED, which is bidirectional.

Table S4

materials	thickness (nm)	
TiO$_2$	19	
SiO$_2$	89	⎫
TiO$_2$	52	⎬ 15 periods
SiO$_2$	63	
TiO$_2$	66	
SiO$_2$	73	⎫
TiO$_2$	42.5	⎬ 22 periods
SiO$_2$	154	
GaAs substrate	-	

Table S4. Structure of the multilayered dielectric optical filter deposited on GaAs.
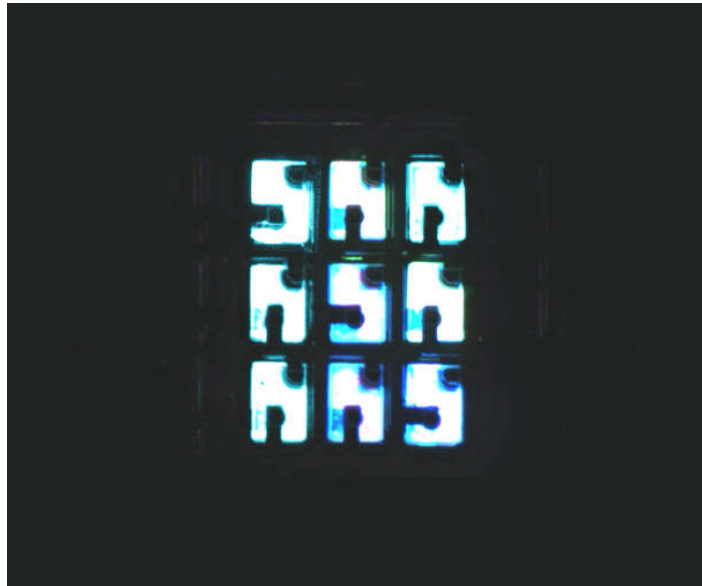
Movie S1

Movie S1. Video for a single pixel of tandem RGB micro-LEDs assembled on a polyimide substrate, displaying different colors under current injection.

Movie S2

Movie S2. Video for an array of tandem RGB micro-LEDs forming a seven-segmented display, showing various decimal numerals.

Movie S3

Movie S3. Video for a 3 × 3 array of tandem RGB micro-LEDs, displaying various colored patterns.